ESD-TDR-65-54

Technical Note

1965-5

Proposed Electronic Systems for the LES Radiation Experiment (September 1964)

J. H. Binsack

20 July 1965

Prepared under Electronic Systems Division Contract AF 19(628)-5167 by

Lincoln Laboratory
MASSACHUSETTS INSTITUTE OF TECHNOLOGY
Lexington, Massachusetts

The work reported in this document was performed at Lincoln Laboratory, a center for research operated by Massachusetts Institute of Technology, with the support of the U.S. Air Force under Contract AF 19(628)-5167.

MASSACHUSETTS INSTITUTE OF TECHNOLOGY

LINCOLN LABORATORY

PROPOSED ELECTRONIC SYSTEMS FOR THE LES RADIATION EXPERIMENT (SEPTEMBER 1964)

J. H. BINSACK

Group 63

TECHNICAL NOTE 1965-5

20 JULY 1965

LEXINGTON MASSACHUSETTS

ABSTRACT

To study the electron radiation environment of the Lincoln Experimental Satellite (LES), an electron detecting telescope has been proposed by C. Mack, et al. This report presents the proposed electronic system for this radiation experiment. This system is the result of a summer study by the author.

The logical design of the electronic system is based on the use of a "hybrid counter" as the scaler. The "hybrid counter" employs the best features of both the "fixed time" and the "fixed count" scalers and can operate over a wide range of counting rates.

Coincidence logic is programmed within the experiment so that the telescope can monitor the electron flux for energies from 60 Kev to 10 mev with counting rates from 100,000 counts/sec down to 0.1 count/sec.

The design of a charge sensitive solid state preamplifier and measurement chain is detailed. The integrating and differentiating time constant is set at 0.5μ sec, and a noise linewidth of 27 Kev (fwhm) is achieved at 30°C with a simulated input capacitance of 100pf.

Accepted for the Air Force
Stanley J. Wisniewski
Lt Colonel, USAF
Chief, Lincoln Laboratory Office

This was sent to PIO to check on Public release. — OK received 29 Sep 65 — Wreck, TS4 / 4 Oct 65

TABLE OF CONTENTS

I. INTRODUCTION

The purpose of the Radiation Experiment on the Lincoln Experimental Satellite (LES) is to measure the spatial and temporal variation of the energy spectrum of high energy electrons which will constitute the orbital radiation environment of the LES.

The experiment was divided into two areas with separate teams responsible for the effort in these areas:

a) C. Mack, J. Ryan, and A. Stanley studied the feasibility of the experiment. They established the physics concept of the experiment, and the detector characteristic, quality and configuration for the detection of energetic electrons.

b) J. Binsack and R. E. McMahon studied the implementation of the experiment. They established the experiment parameters, and the electronic system characteristics, quality and configuration from the processing of the detector outputs to the presentation of data to the telemetry system.

This report summarizes the three-month summer study conducted by the author, and represents the experiment parameters and electronic system design as presently configured.

II. ANALYSIS OF THE EXPERIMENT

A. General

The general ground rules for the experiment were outlined in early June 1964 as the following:

1) Solid state detectors would be serially stacked in a constant solid angle configuration.

2) Coincidence schemes would be used to determine how deep into the stack an energetic particle had penetrated. This is indicative of its initial energy.

3) The energy range of interest was the spectrum from 100 kev to 10 Mev for electrons. No interest was expressed for protons.

4) Due to radiation damage within the detectors caused by

accumulated dosage of high energy particles, the maximum rate of arrival of particles would be limited by the configuration geometry to 10^4 - 10^5 counts/sec. Thus the accumulated dose for a year's time would not cause the detectors to deteriorate.

5) A complete measurement sequence should take less than 40 seconds to avoid any significant spatial and/or temporal variations within the data sequence.

With these guidelines and as other information became available a system was evolved which will be discussed in the following sections.

B. Detector Signal Analysis

When an energetic particle passes through a solid state detector, it loses energy in ionizing collisions, bremsstralung and several other loss mechanisms. Roughly 3.5 e v are lost in each ionizing collision within a silicon detector.

Electrons differ from protons and other heavy particles in that they are not characterized by straight-line paths and definite ranges. Rather, the electron paths are quite tortuous, and the ranges of monoenergetic electrons vary greatly. Evans* states that only 3% of the flux of monoenergetic electrons have sufficiently straight paths to penetrate an absorber whose thickness is equal to the mean path length $\overline{S}$. The crooked paths are due to the multiple scattering with atoms along the paths. Scattering may take place in collisions with orbital electrons or with the nuclei of the absorbing material. The variation in the ranges of monoenergetic electrons is due primarily to the crooked paths followed by the particles. Here range means the distance which the electron penetrates, measured parallel to the initial direction of the electron.

---

*R. D. Evans, The Atomic Nucleus (McGraw-Hill, New York, 1955).

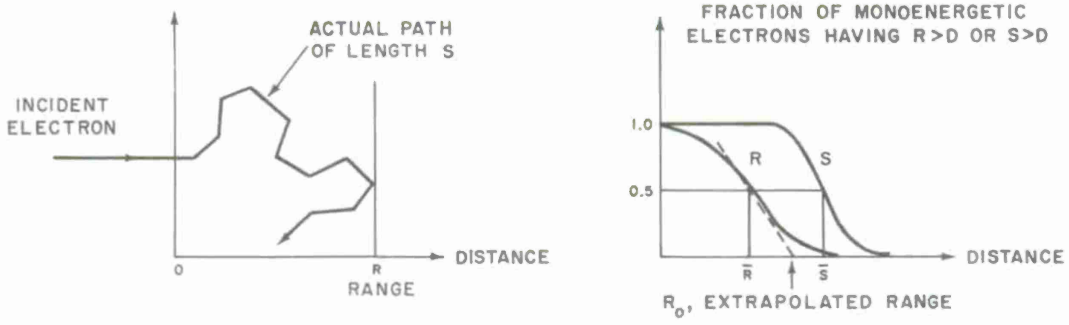

Various curves are available which give the ranges of electrons in silicon. Figure 1 shows the average range, while Fig. 2 illustrates the maximum range. Figure 3 gives the amount of energy lost in silicon detectors of various thickness.

The scattering, straggling and range variation problems are well illustrated by the data depicted in Figure 4. Here one finds that all the particles with energies below 350 kev are completely stopped by the detector, as they should be. However, very many of the higher energy particles are scattered sufficiently to deposit all their energies in the detector. There is a total absorption peak even up to 1.2 Mev, whereas the curves of average ranges would indicate that all these particles should pass through the detector as minimum ionizing particles and deposit only about 180 kev within the detector. Furthermore, the mean multiple scattering angle is about 30° for 1.8 Mev electrons.

The lack of an adequate theory and reliable empirical data underlines the necessity of careful and extensive testing and calibration of an experiment to measure electrons with solid state detectors.

For the purpose of arriving at the experiment parameters the curves of Figure 1 and Figure 3 were assumed to be adequate, and these were used

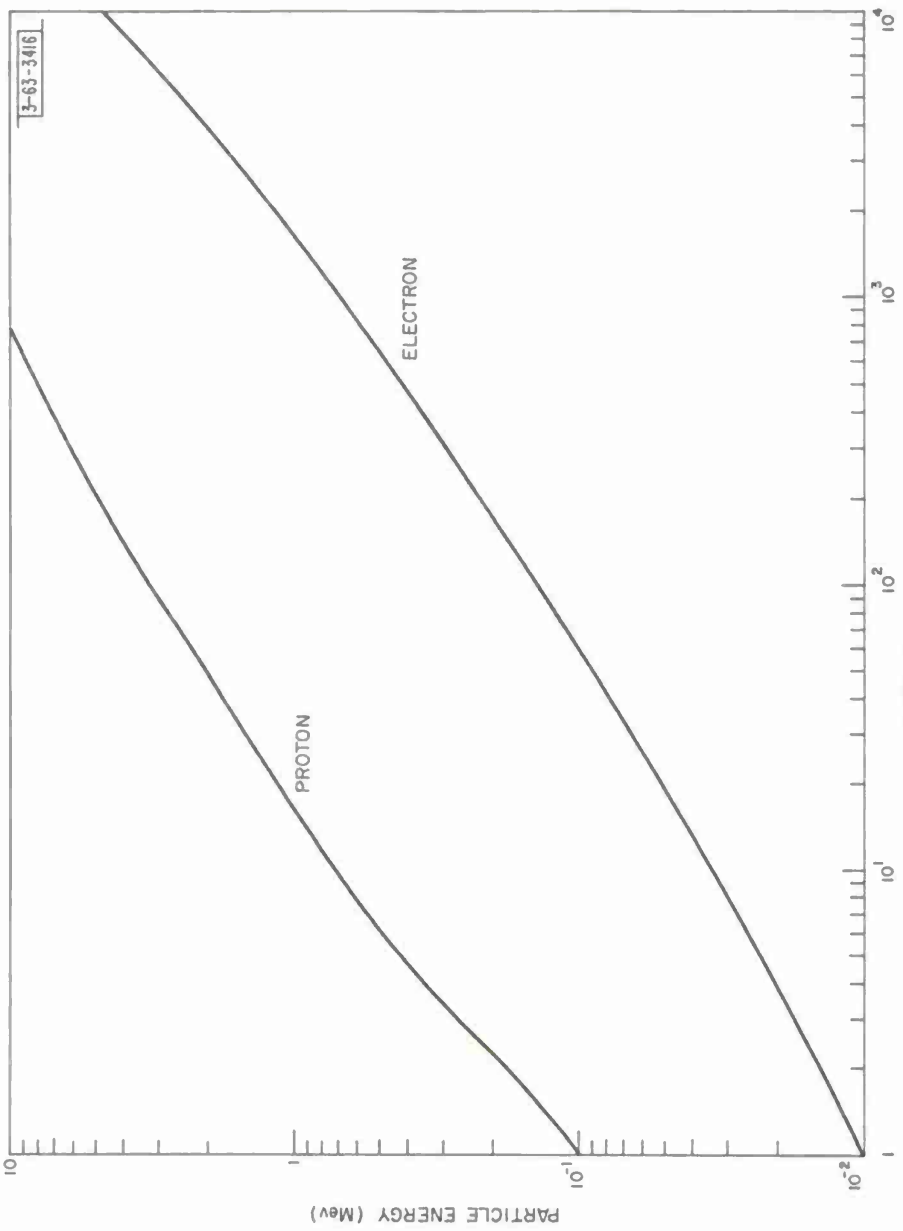

Fig. 1 Ranges in Silicon

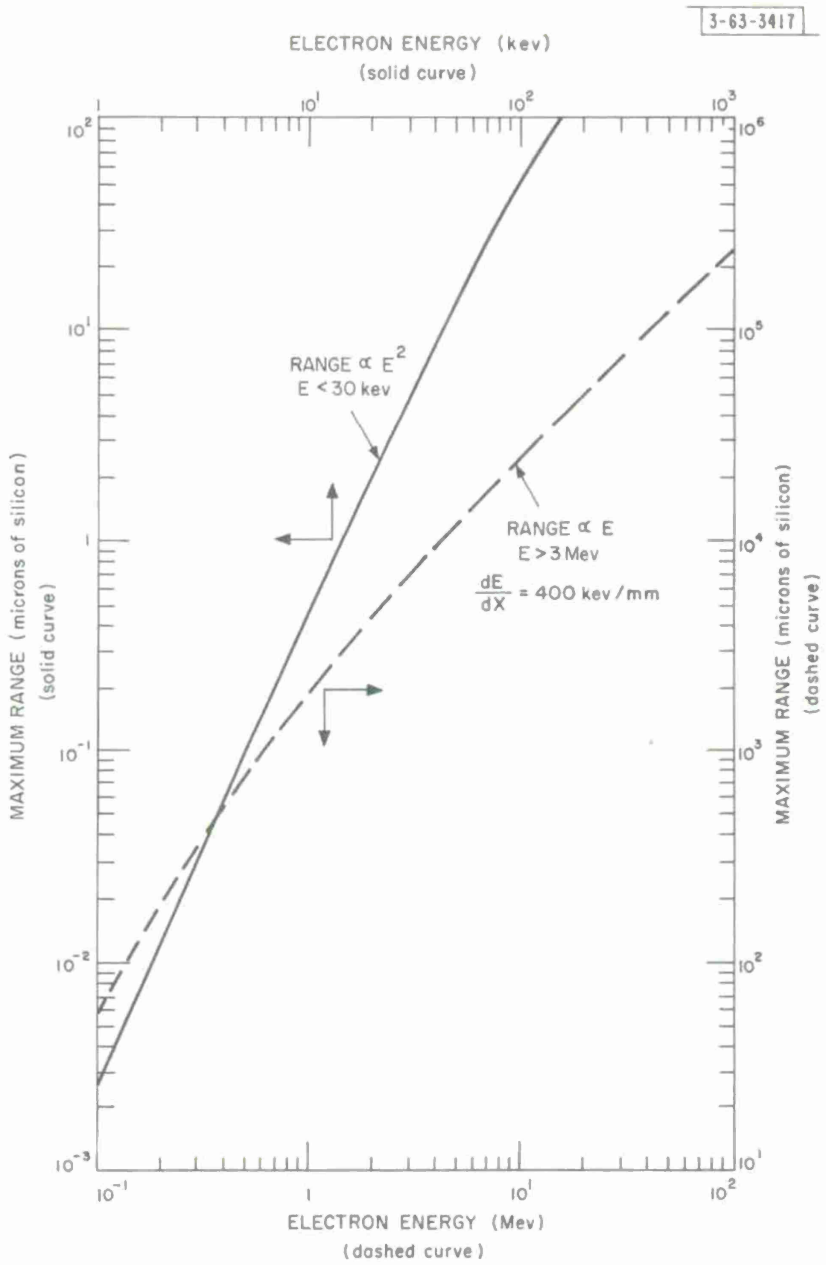

Fig. 2 Range-Energy Curves for Silicon

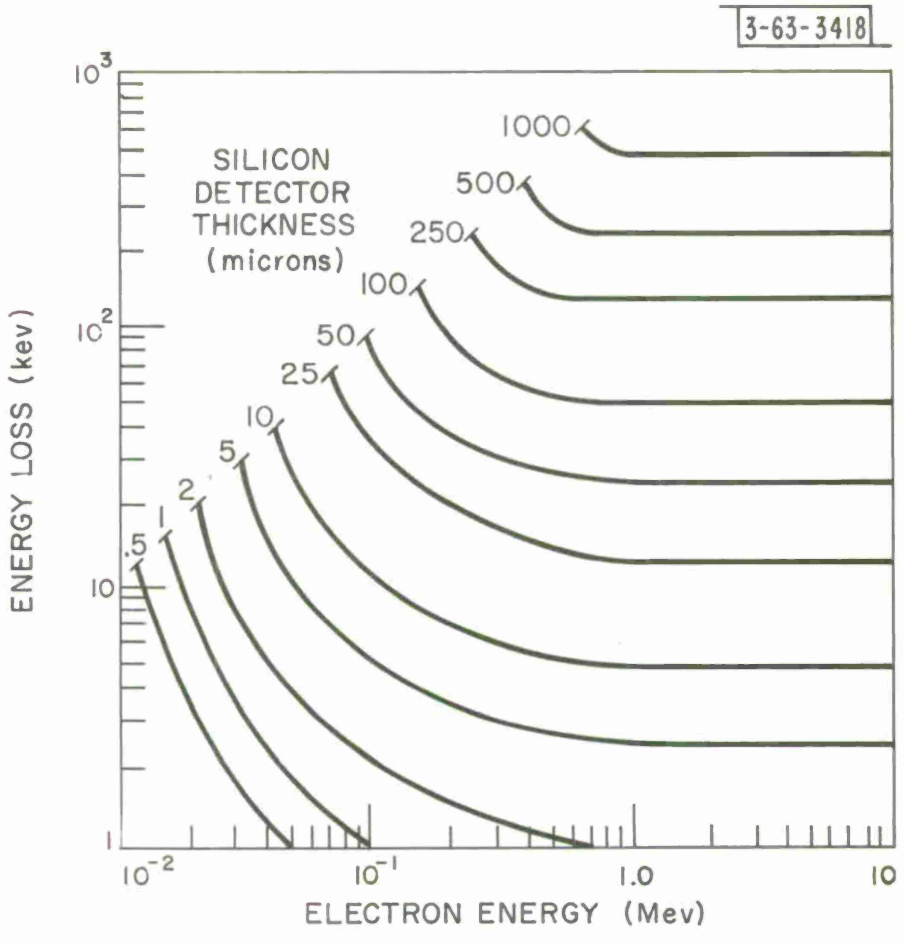

Fig. 3 Electron energy absorption in thin silicon detectors.

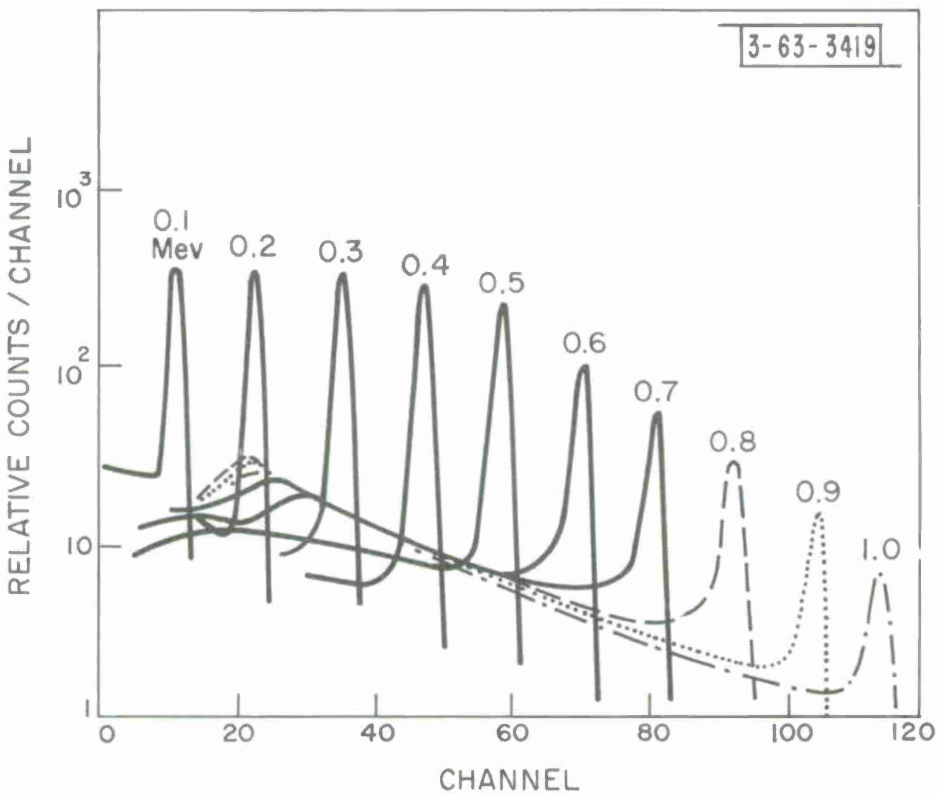

Fig. 4 The response of a 12,000 ohm-cm diffused junction silicon counter to equal numbers of monoenergetic electrons in the range 100 Kev to 1 mev. At a detector bias of 200 v. The thickness of the depletion layer corresponds to the range of an electron of energy 350 Kev. (McKenzie and Ewan, IRE Trans. Nucl. Sci. NS-8, #1, 50, 1961.

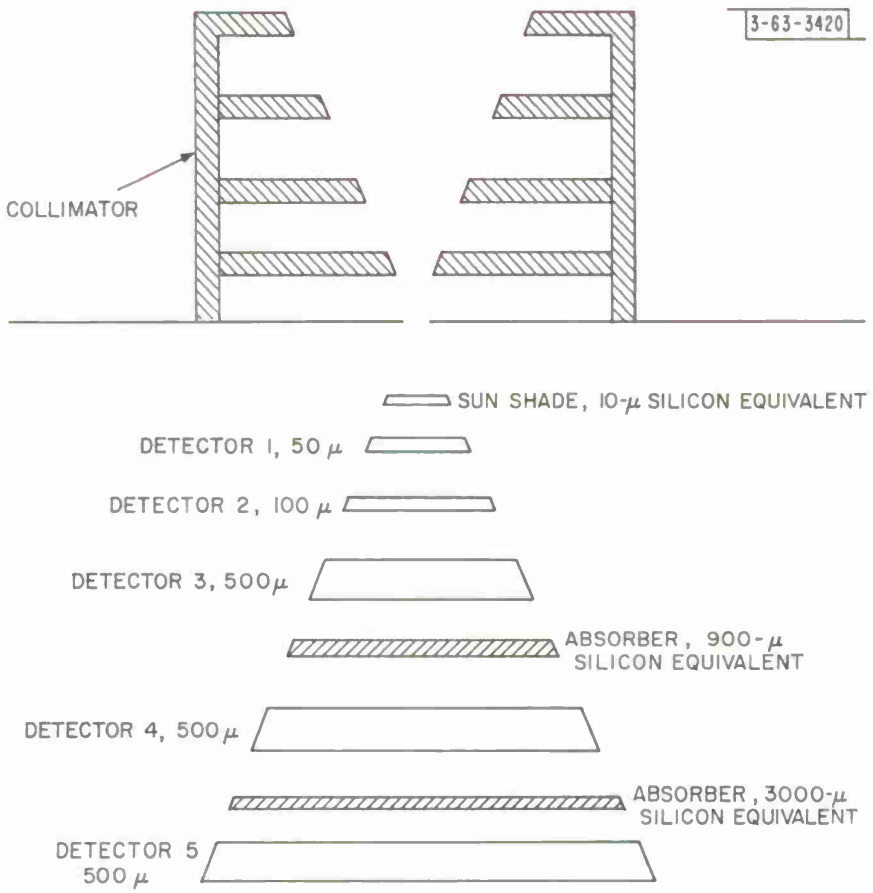

Fig. 5 Detector Configuration (schematic illustration)

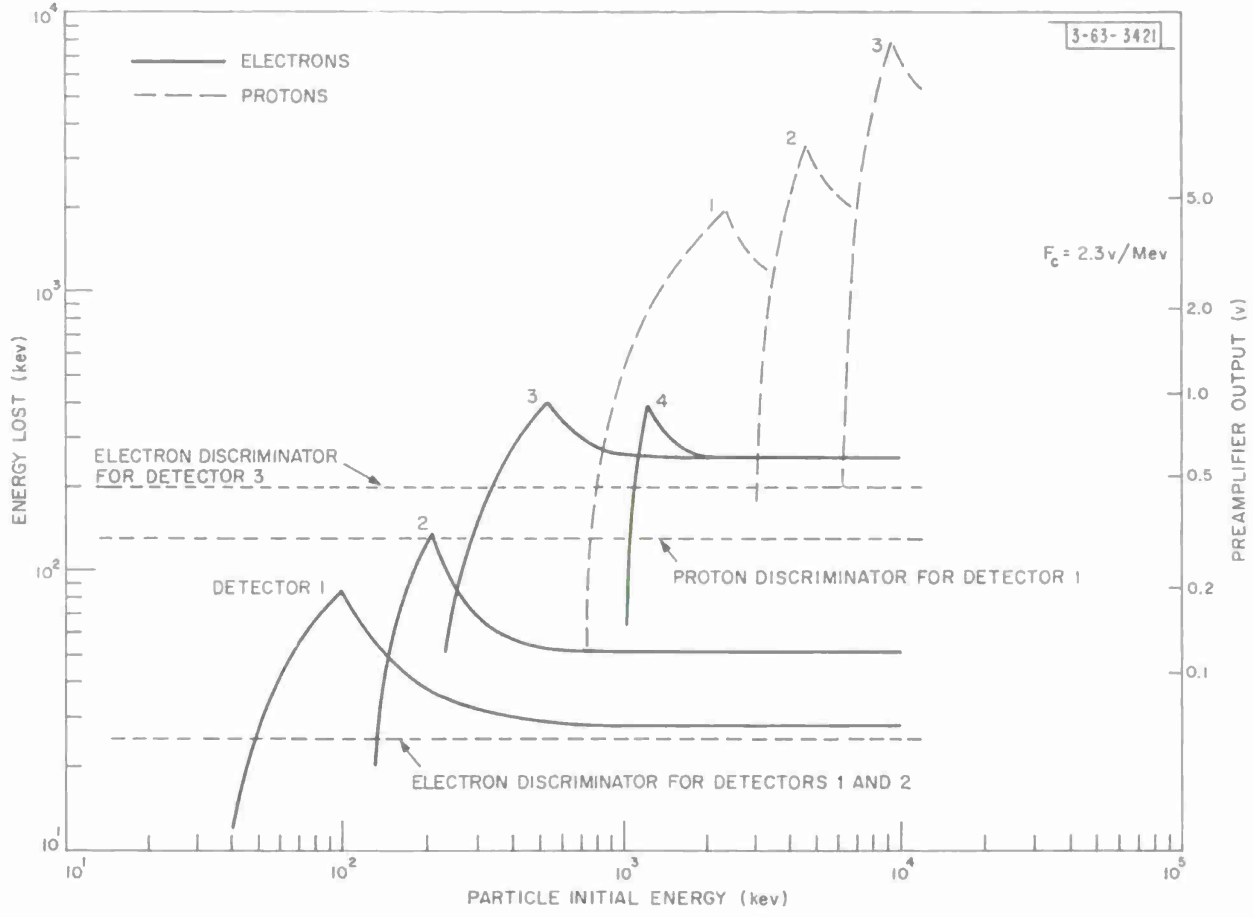

Fig. 6 Energy Relations for a Particular Detector Stack

in the following analysis.

Of primary concern in the system design is the size of the signal from each detector. The approach taken was to compute the amount of energy lost in each detector as a particle of a given initial energy passed through the stacked detectors as illustrated schematically in Figure 5. The sun shade is to prevent any direct photoelectric effect that external light may have on the detectors. The shade also serves to stop protons with energies below 740 kev, and electrons with energies below 35 kev.

Figure 6 consolidates the results of the computations which are illustrated in the following example:

> Let an electron with initial energy of 300 kev be incident normal to the detectors, and assume its path through the detectors is straight and parallel to its initial direction. From Figure 3 it is seen that a 300 kev electron wil lose 5 kev in the sun shade and thus emerge with 295 kev. The electron with this energy will lose about 30 kev in the 50 microns of the first detector (see Figure 6). Now the back region of detector #1 and the front layers of detector #2 constitute a so-called "dead layer" of useless absorber. For the detectors chosen it is unclear what this depth is, so that an assumed dead layer of 25 microns is used. The electron emerging from the rear of the depletion layer of detector #1 has about 265 kev and will lose another 25 kev in the dead layer.
>
> In the 100 microns of the second detector the 240 kev electron will lose about 70 kev and then, as a 170 kev electron lose 25 kev in the dead layer between the back of detector #2 and the front of detector #3. The electron now has 145 kev as it approaches the depletion layer of detector #3, where it will deposit all its energy.

Summary of the example:

Initial energy		E_i = 300 kev
Energy lost in Det.	#1	≈30 kev
	#2	≈70 kev
	#3	≈145 kev
	#4	≈0
	#5	≈0

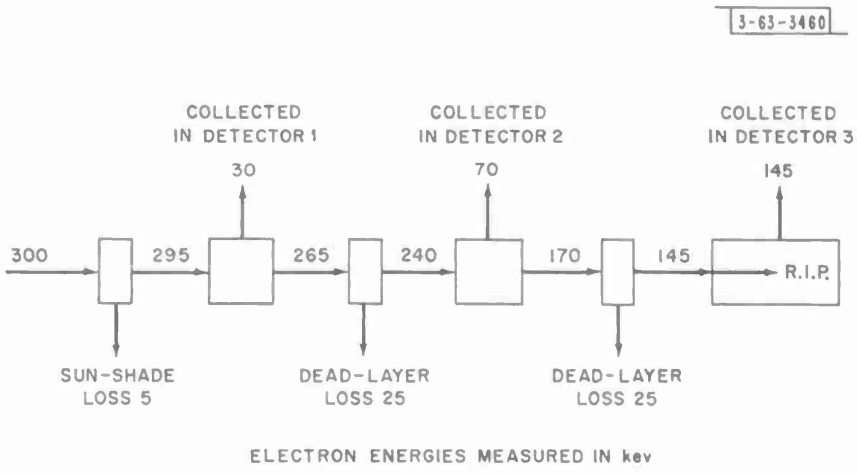

The distinction between electrons and heavier particles can be made easily in the first detector. Protons and heavier particles will deposit a significantly larger amount of their energy in this detector and the correspondingly larger signal can easily be discriminated as can be seen from Figure 6.

The properties of the absorber between the fourth and fifth detectors have not been specified at the time of this writing and thus the energy lost in the fifth detector as a function of the particle's initial energy cannot be computed.

The next topic to be considered is the choice of the coincidence logic in the measurements based on a statistical analysis of the expected signals.

C. Statistical Analysis of the Measurement Process

The full statistical analysis of the measurement process is beyond

the scope of this report* For the purposes of this discussion the following assumptions are made concerning the processed signals from the detector:

1) The amplitude of the signal alone is directly proportional to the amount of energy lost by the particle in the detector; i. e. Figure 6 applies.
2) The signals are non-overlapping. This will be sufficiently true if the arrival rate is low enough, and the response characteristics of the measurement chain are properly designed.
3) The amplitude of the signal is corrupted by additive Gaussian noise.
4) The discriminators can be set at an arbitrary level and are constant.

With these assumptions the analysis begins by measuring the noise contribution from the preamplifier. It has been found to be 27 kev full width half maximum (fwhm) at T = 30°C and a simulated detector capacity of 100 pf (see Section IV-F). The noise contribution from the detector itself is quoted as 16 kev fwhm by Ortec. Thus the total input noise is $(27^2 + 16^2)^{1/2} = 31.4$ kev fwhm. For Gaussian noise the ratio of fwhm to rms is 2. 35. Therefore, the 1 σ value of the noise is 13. 3 kev.

The discriminator level for the second detector is set at 25 kev which is half the 50 kev expected from high energy electrons. Thus there will be an equal number of false counts as missed counts as a result of the symmetrical properties of additive Gaussian noise. It is anticipated that the second discriminator will be the enabling gate for all the coincidence logic, and thus this symmetry property is desirable.

The other discriminators are set at levels to give adequate noise discrimination for the signal levels expected. A proton discriminator

*It appears that the type of random process involved here is a non-homogeneous (time varying) Poisson derived (the effects of straggling and scattering) process with unknown arrival rate, corrupted by additive white Gaussian noise (preamp and detector) and filtered by the measurement chain.

monitors the output of detector #1 and distinguishes large signals due to the energy lost by protons or heavier particles. This discriminator level is set at 130 kev so that total absorption electrons which lose more than this energy will not be counted incorrectly as low energy particles.

These features are clearly illustrated in Figure 7, which indicates the probability that a particle which loses , E_{lost}, in a detector will trigger the associated discriminator. By convolving this graph with that of Figure 6 one can determine the probability that a particle with initial energy, E_i, will trigger a particular detector's discriminator, Figure 8.

From this data a decision was made on what measurements were to be performed based on a high probability of registering coincidence counts for that particular measurement. The proposed measurements include four differential measurements and four integral measurements synthesized by various logical combinations of the discriminator outputs. These are summarized in Table I and the probability of registering counts during these measurements is shown in Figures 9 and 10.

III. DESIGN OF THE EXPERIMENT

A. General

The block diagram electronic system designed to accomplish the desired measurements is shown in Figure 11. It consists of five stacked detectors each with its own measurement chain and discriminator. The extra proton discriminator, l_p, associated with detector #1 is also indicated. A sixth detector, measurement chain and discriminator monitors the effect of the experiments environment on a detector, by being exposed to a source of known intensity.

The outputs of the discriminators pass into the appropriate coincidence logic to form the necessary levels required during the various measurements. The output then is processed in a Hybrid Counter which contains the information to determine the rates for each measurement. Hybrid Counter #1

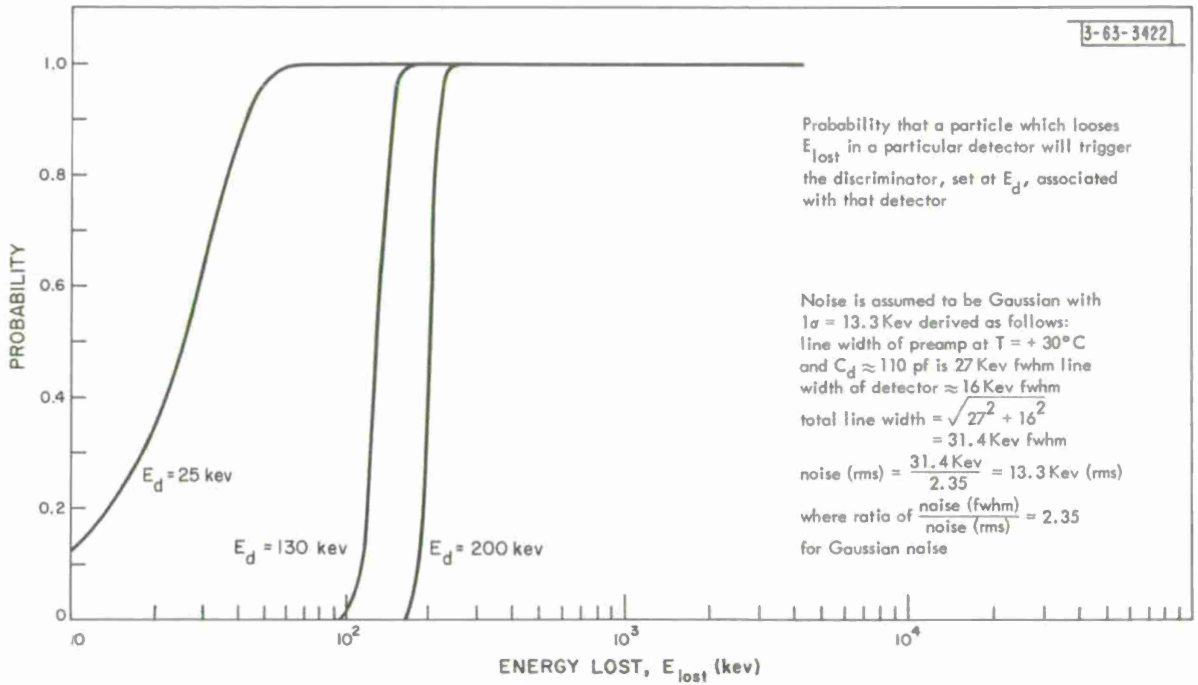

Fig. 7 Discriminator Probability Curve

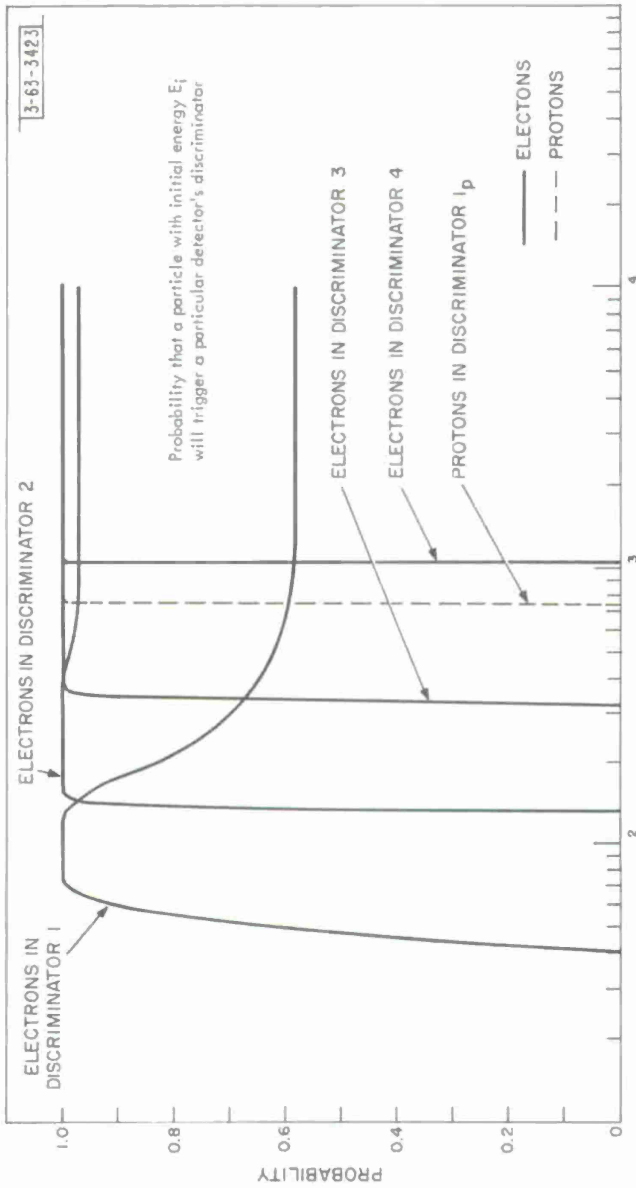

Fig. 8 Discriminator Probability Curve

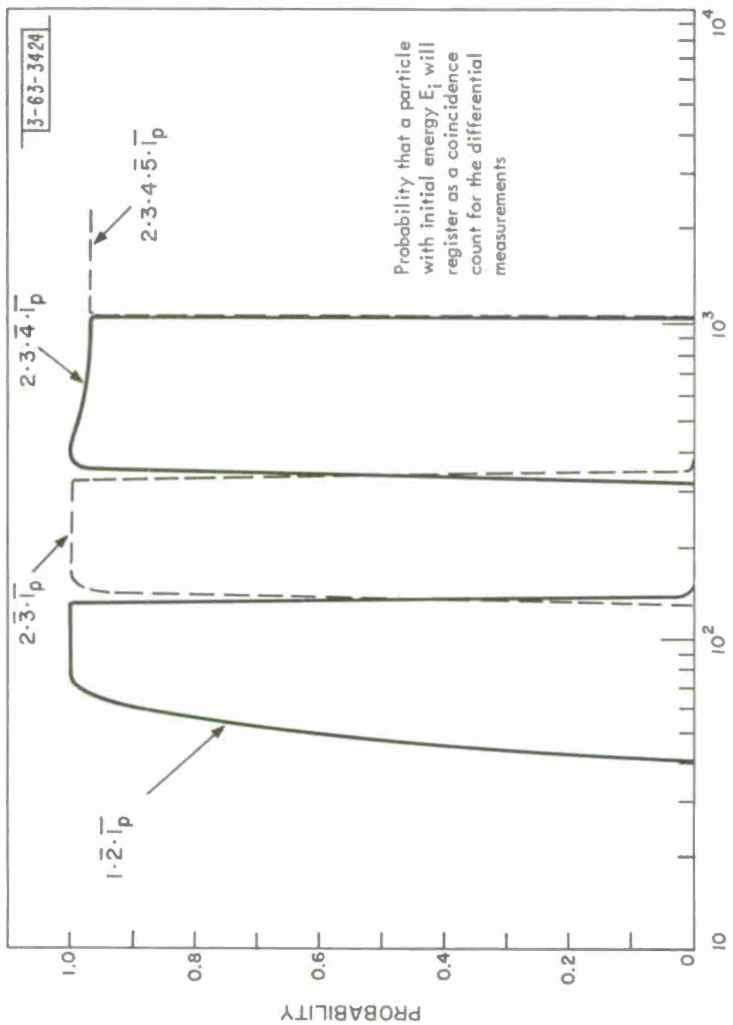

Fig. 9 Discriminator Probability Curve

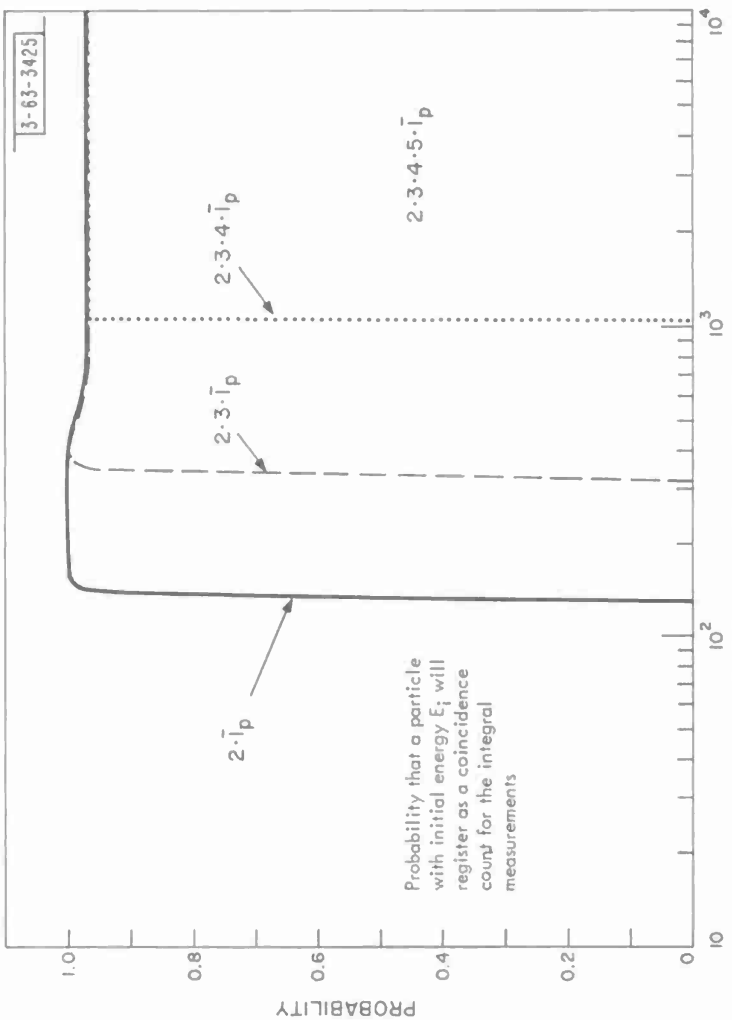

Fig. 10 Discriminator Probability Curve

TABLE I

DIFFERENTIAL MEASUREMENTS

	Discriminators required to be in logical coincidence	Measurement determines flux of electrons within an Energy Band
M_1	$1 \cdot \overline{2} \cdot \overline{I}_p$	40 - 60 kev < E < 130 kev
M_2	$2 \cdot \overline{3} \cdot \overline{I}_p$	140 kev < E < 330 kev
M_3	$2 \cdot 3 \cdot \overline{4} \cdot \overline{I}_p$	350 kev < E < 1 Mev
M_4	$2 \cdot 3 \cdot 4 \cdot \overline{5} \cdot \overline{I}_p$	1 Mev < E < (unknown at this time)

INTEGRAL MEASUREMENTS

	Discriminators required to be in logical coincidence	Measurement determines flux of electrons with Energies greater than a specified energy
M_6	$2 \cdot \overline{I}_p$	140 kev < E
M_7	$2 \cdot 3 \cdot \overline{I}_p$	350 kev < E
M_5	$2 \cdot 3 \cdot 4 \cdot \overline{I}_p$	1 Mev < E
M_8	$2 \cdot 3 \cdot 4 \cdot 5 \cdot \overline{I}_p$	(unknown at this time) < E

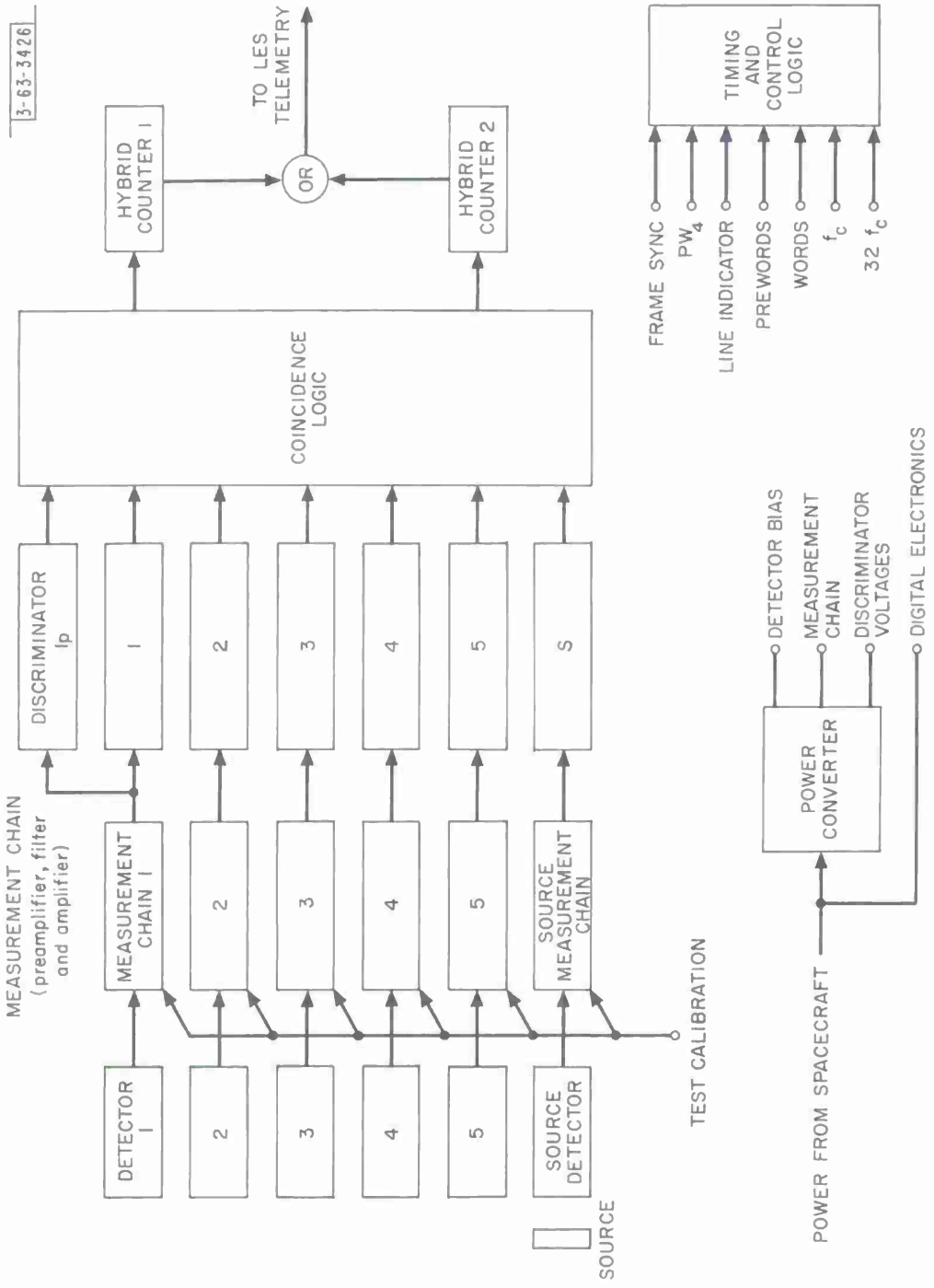

Fig. 11 Block Diagram of Radiation Experiment

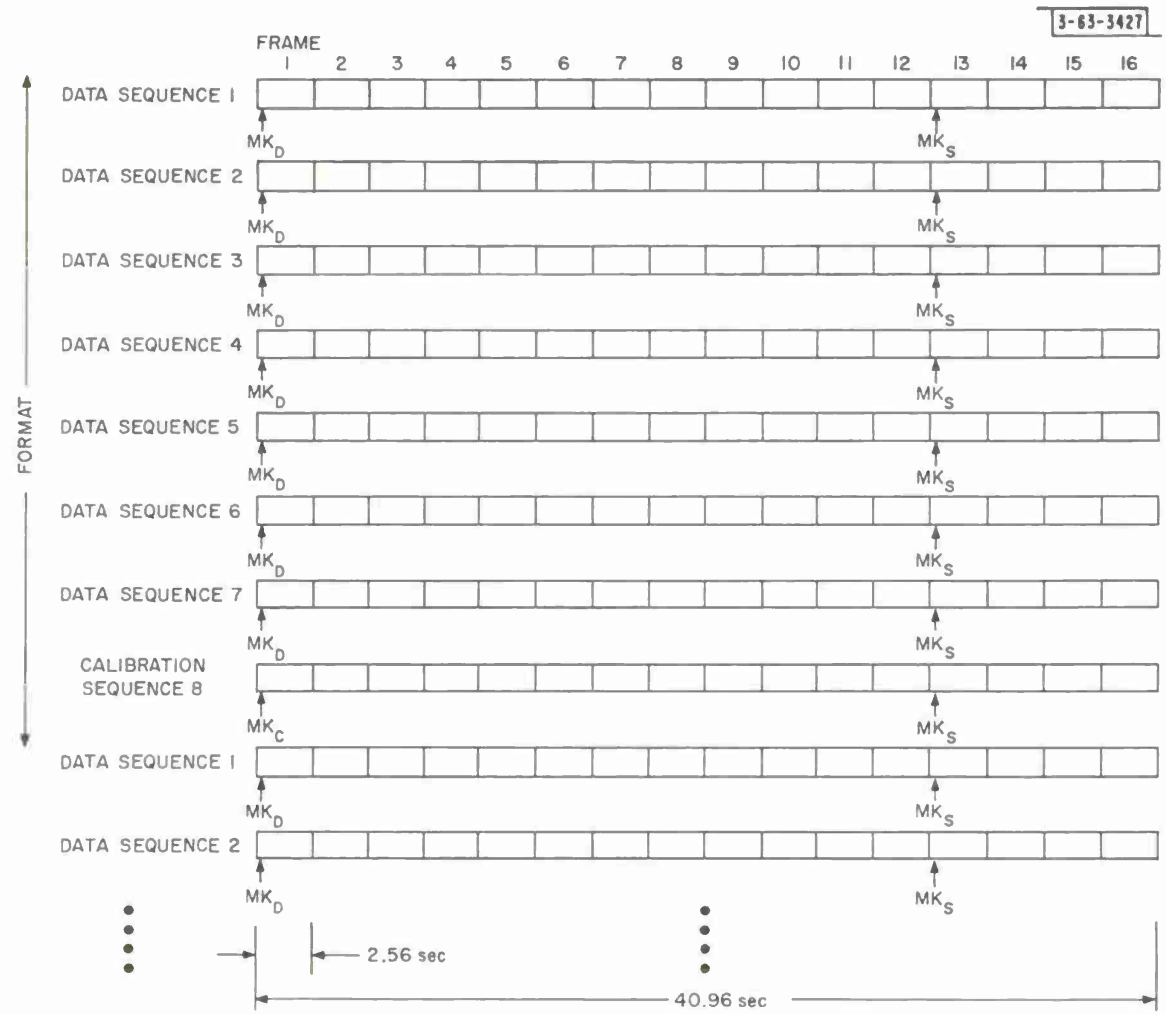

Fig. 12 Format for Radiation Experiment

is time shared among the four differential measurements, three integral measurements and the source measurements. Hybrid Counter #2 is not time shared, but is devoted exclusively to the long duration integral measurements ($2 \cdot 3 \cdot 4 \cdot 5 \cdot \overline{I}_p$).

The system is run synchronously with the LES telemetry system; the timing and control logic is all derived from signals supplied from the telemetry package. A power converter appears to be required to supply the roughly -200 volt reverse bias on some detectors. This converter may also be used for regulating and filtering the supply voltages in the measurement chain and discriminators.

B. Format of the Experiment

The basic format of the experiment (the longest cyclic period) contains 8 sequences. Each sequence is 40.96 sec. long and is the period during which one entire measurement sequence is completed, i.e. four differential, four integral and a source measurement are made during a single sequence.

The 8 sequences within a format are divided into 7 data gathering sequences, and 1 calibration sequence, see Figure 12. During the calibration sequence, the detectors are electrically removed from the inputs of the measurement chains (by disabling their bias voltage), and known charges are simultaneously deposited at the inputs to every measurement chain. The charges are derived from a voltage step at a submultiple of the available clock frequency. The resulting discriminator outputs are processed through the coincidence logic and applied to Hybrid Counters. It should be noted that, because all discriminators are being triggered simultaneously in this mode, any count registered during a differential measurement is a false count, and thus indicative of the systems error rates. Furthermore, since the charges are derived from a clock frequency, the counts registered during the integral measurements should be constant. Any deviation from these constant numbers is again indicative of the systems error rates. In this way the entire electronic system can be calibrated and tested as an integral part of the operating format.

Before preceding into the details of the data sequence, it is desirable to discuss the features of this Hybrid Counter. In the course of this discussion, the parameters required for its use in this experiment are developed. These parameters then determine the arrangement of the measurements within the data sequence.

C. The Hybrid Counter

1. Rate Determination Concepts, and the Hybrid Counter

There exists two classical methods of determining the rate of arrival of random events:

a) Fixed Time: Within a specified time, T_o, determine the number of events, $N(T_o)$, which have occurred. The rate is then $R_a = \frac{N(T_o)}{T_o}$ events/sec.

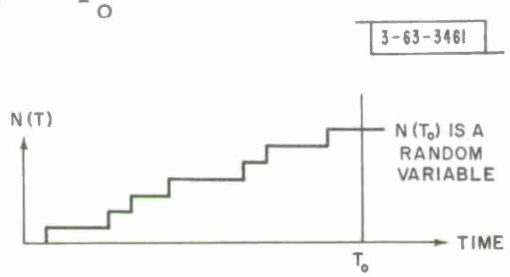

b) Fixed Count: Determine the time, T, required to accumulate a specified number of events, N_o. The rate is then $R_b = \frac{N_o}{T}$ events/ sec. This determination is normally accomplished by counting the number, N_c, of clock periods (T_c) until $N(T) = N_o$. The rate is $R_b = \frac{N_o}{N_c T_c}$ events/sec.

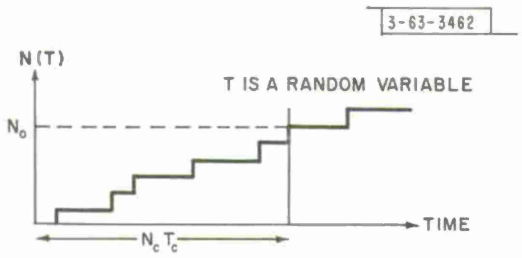

Method (a) requires a counter whose length is determined by the expected upper limit of the rate, since it must then be capable of a large count within the specified time, T_o. The relative error in the determination of the actual rate is inversely proportional to that rate.

$$\epsilon = \frac{dR_a}{R_a} = \frac{dN(T_o)}{N(T_o)} = \frac{1}{R_a}\,\frac{dN(T_o)}{T_o} = \frac{1}{R_a}\,\frac{100\%}{T_o}$$

since dN is a unit quantum.

Method (b) requires a counter whose length is determined by the expected lower limit of the rate, since it must be capable of counting a large number of clock periods until N_o events have occurred. The relative error in the determination of the actual rate is directly proportional to that rate.

$$\epsilon_b = \frac{dR_b}{R_b} = -\frac{dT}{T} = -\frac{T_c\,dN_c}{N_o}\,R_b;\ |\epsilon_b| = R_b\,\frac{100\,T_c}{N_o}\ \%$$

since dN_c is a unit quantum.

Thus, on the one hand, the relative error decreases at higher rates, (fixed time); and one the other hand, the relative error increases at higher rates (fixed count). Unfortunately, in most applications, there is a specified nominal rate, R_n, which is to be verified accurately, with expected variations both above and below the nominal rate. Furthermore, it is desirable to determine these deviations with an error that is a minimum at the nominal rate, and which increase symmetrically both above and below this nominal rate.

3-63-3463

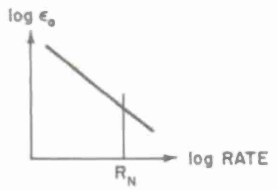

"FIXED TIME" ERROR

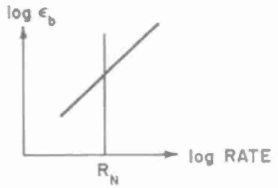

"FIXED COUNT" ERROR

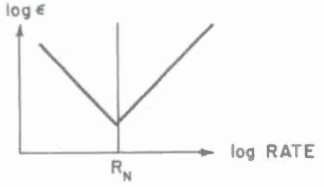

DESIRED ERROR

Fortunately, there is a method of combining the best features of both the "Fixed Time" and "Fixed Count" schemes into a single counter which can minimize the error at the nominal rate.

This Hybrid Counter* counts the number of occurrences of random events for a specified time, T_o. If the nominal rate is exceeded, then a number $N_o = R_n T_o$ will be reached at time T, prior to time T_o. The mode of operation of the counter is then changed at time T so as to count the number, N_c, of clock periods (T_c) that occur between times T and T_o. Thus the same counter can operate in two distinct modes:

a) Low Rate Mode: The rate of occurrence of random events is lower than the nominal rate. The number, N, of random events occurring in time T_o is less than or equal to $N_o = R_n T_o$.

$$\text{Low Rate: } R_L = \frac{N}{T_o} \leq R_n = \frac{N_o}{T_o} \text{ events/sec}$$

$$\text{Low Rate Error} = \frac{dR_L}{R_L} = \frac{1}{R_L} \quad \frac{100}{T_o} \ \%$$

3-63-3464

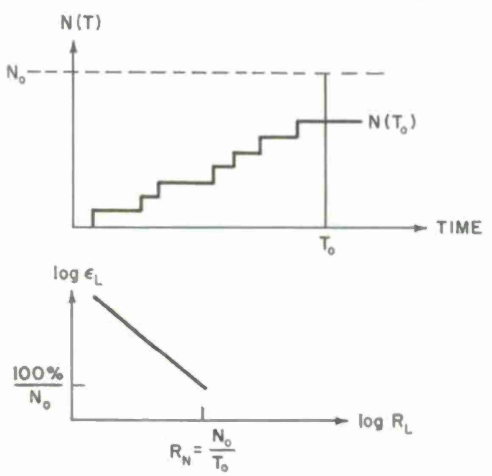

*This counter is similar to the one used in the Gamma Ray Telescope, as described by W. G. Schmidt.

b) High Rate Mode: The rate of occurrence of random events exceeds the expected nominal rate. N_o events have occurred in a time T shorter than T_o. The number, N_c, of clock periods within the time remaining between T and T_o is counted. In actual practice it is convenient to introduce a parameter, K, which extends the duration of the clock period to K T_c.

$$\text{High Rate: } R_H = \frac{N_o}{T} = \frac{N_o}{T_o - N_c K T_c} \geq R_n = \frac{N_o}{T_o} \text{ events/sec}$$

$$\text{High Rate Error: } \epsilon_H = \frac{dR_H}{R_H} = R_H \frac{100\ K\ T_c}{N_o} \ \%$$

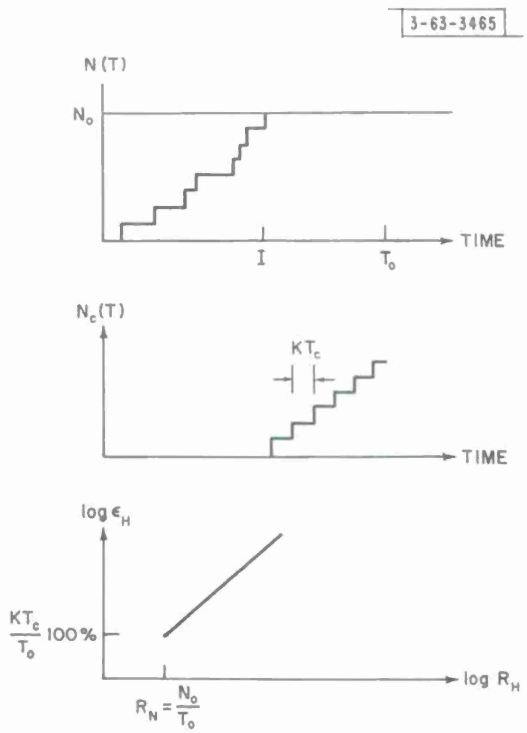

The general synthesis of a Hybrid Counter is shown below.

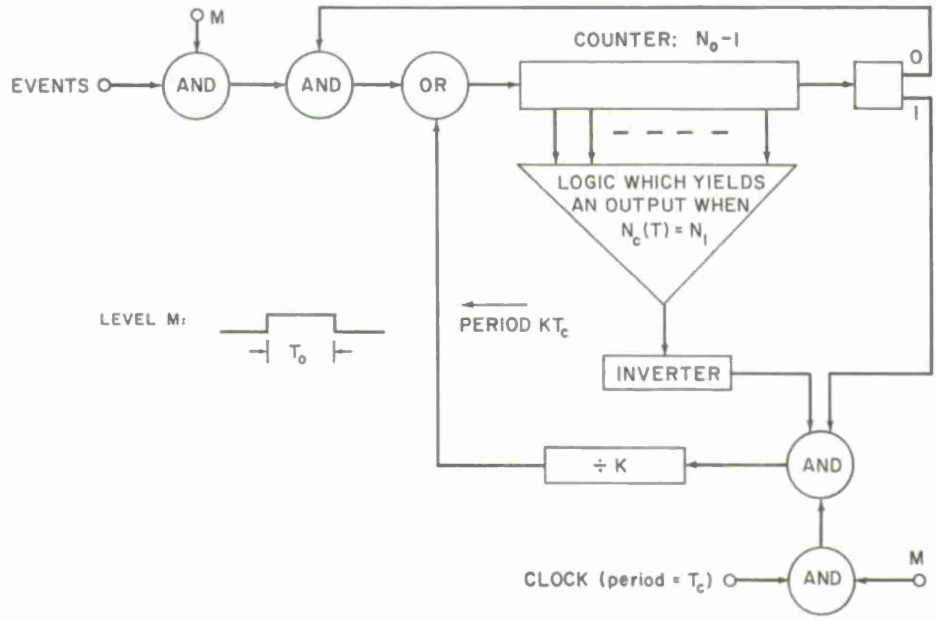

It should be noted that at the time the Hybrid Counter enters the High Rate mode, it is automatically in a state such that $N_c(T) = 0$, and thus pulses with period $K T_c$ can be counted immediately without resetting the counter. As a precaution against an ambiguous interpretation of the contents of the counter, the counter is prevented from overflowing a second time due to excessive counting of clock derived pulses. This is done by merely establishing an upper limit to N_c, call it N_1, which if reached inhibits any further counting during the period T_o. Normally, it is desirable (and easy) to choose parameters such that $N_1 K T_c \geq T_o$ which implies that N_1 will never be reached and that the maximum rate in the high mode approaches infinity.

2. Application of the Hybrid Counter to the Radiation Experiment

The word length of the LES telemetry system is eight bits/word. Thus it is convenient to choose $N_o = 2^7 = 128$, and then to find $T_o = \frac{128}{R_n}$ to achieve the different nominal rates encountered throughout the experiment. The eighth bit is used to distinguish which of the two modes of operation the hybrid counter was in, and thus how the other seven bits are to be interpreted: either as $N(T_o)$ if bit eight is zero; or N_c if bit eight is one.

There are two clock rates supplied from the LES telemetry system, 100 bits/sec and 3.2 K bits/sec. The higher clock rate will be used to define $T_c = 2^{-5} \times 10^{-2}$ sec = .313 milliseconds.

It is also convenient to choose $N_1 = 2^6 = 64$ because if its logical ease (being represented by a single level). Furthermore, any choice of N_1 between 64 and 127 does not influence the final design to a significant degree.

With these parameters:

$N_o = 2^7 = 128$

$N_1 = 2^6 = 64$

$T_c = 2^{-5} \times 10^{-2}$ sec

one may arrive at the following list of useful design relationships:

Nominal Rate: $R_N = \frac{N_o}{T_o} = \frac{128}{T_o}$ events/sec

Low Rate: $R_L = \frac{N}{T_o} \leq \frac{128}{T_o}$ events/sec

Low Rate Relative Error: $\epsilon_L = \frac{1}{R_L} \quad \frac{100}{T_o}$ %

Minimum Error in Low Rate Mode: $\epsilon_L\Big|_{min} = \frac{100}{N_o}$ %

High Rate: $R_H = \frac{N_o}{T_o - N_c K T_c} \leq \frac{128}{T_o - 2 \times 10^{-2} K}$ events/sec

High Rate Relative Error: $\epsilon_H = R_H \frac{K}{4096}$ %

Minimum Error in High Rate Mode: $\epsilon_H\Big|_{min} = R_n \frac{K}{4096}$ %

(occurs at the nominal rate)

It is desirable and easy not to limit the highest rate capable of being registered. Thus if $R_H \to \infty$ then

$$T_o - N_1 K T_c \leq 0$$

or $$\frac{N_o}{R_n} - N_1 K T_c \leq 0$$

Then this restricts the design parameter K so that

$$K \geq \frac{6400}{R_n}$$

With this specification on K then

$$\epsilon_H\Big|_{min} \geq 1.56\ \%$$

Finally for a given percent error the rates are

$$R_L = \frac{100}{T_o \epsilon_L} \quad \text{events/sec}$$

$$R_H = \frac{4096}{K} \epsilon_L \quad \text{events/sec}$$

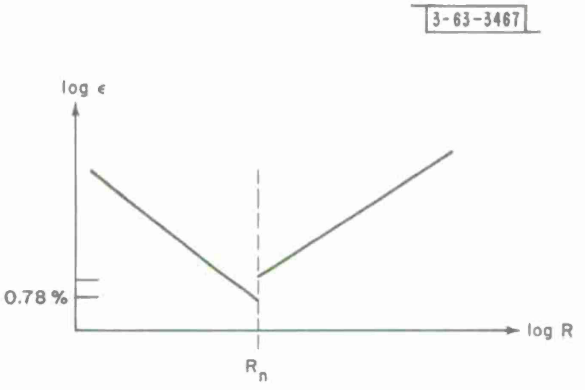

3. Parameters for the Hybrid Counter in the Radiation Experiment

The following is detailed design of the parameters involved in the use of the hybrid counter in the radiation experiment. The terminology used throughout is consistent with that developed for the first measurement, M_1. A summary of the parameters chosen is presented in Table II.

Figures13 and 14 depict the capabilities of the design with regard to the span of rates for each measurement and the relative error associated with determining the actual rates from the available data. Overlaid on these figures is the latest experimental measurements* of the expected electron fluxes in the spatial region of interest. It should be noted that there exists a large temporal variation of the energy spectrum for which allowance must be made.

---

*L. A. Frank, J. A. Van Allen, and H. K. Hills, "The Study of Charged Particles in the Earth's Outer Radiation Zone with Explorer 14," Journal of Geophysical Research, 69, 11, 1 June 1964, pp. 2171 - 2192.

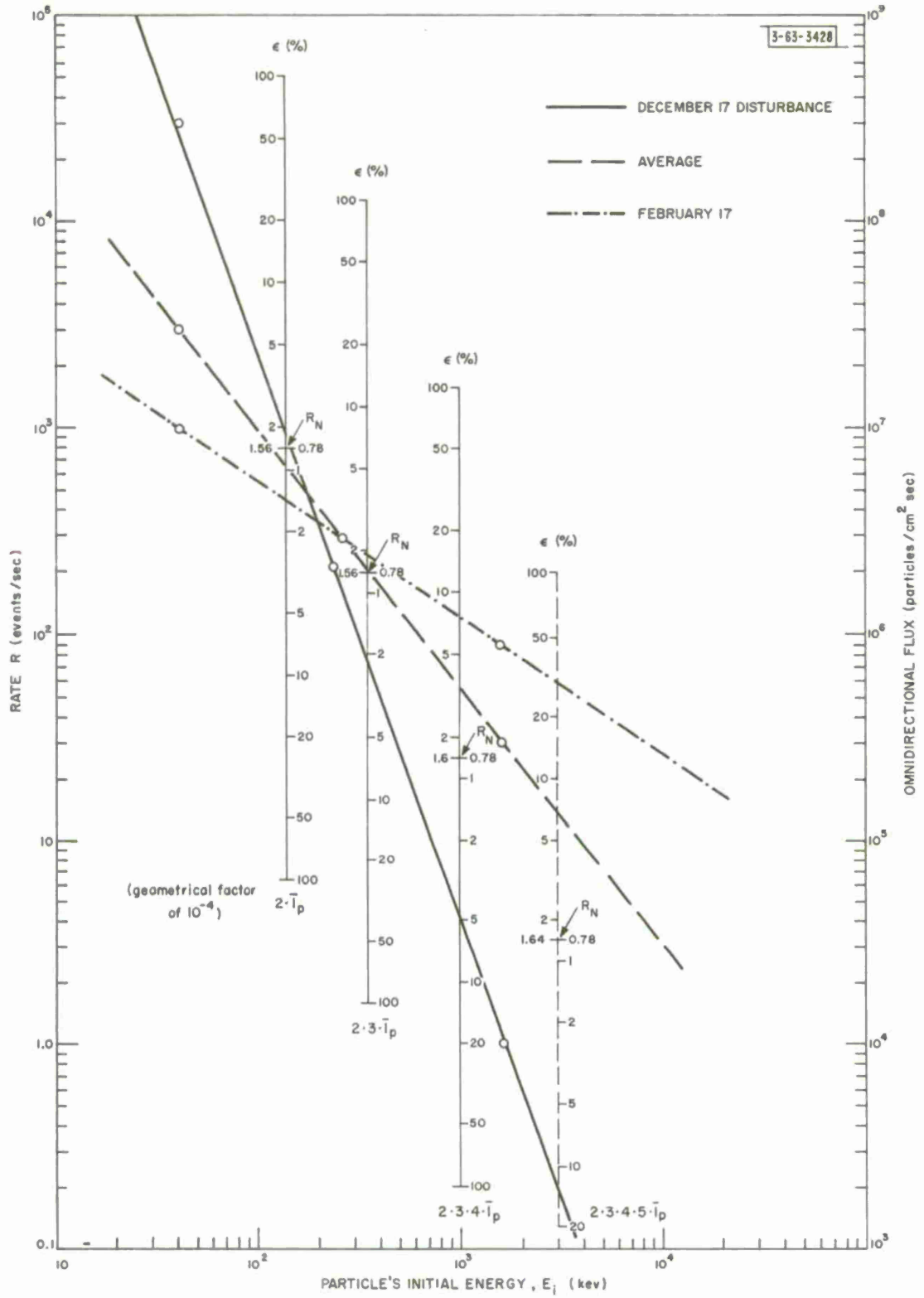

Fig. 13 Integral Measurements. Counting rate vs. particle's energy showing relative error at each rate and previously measured spectrum.

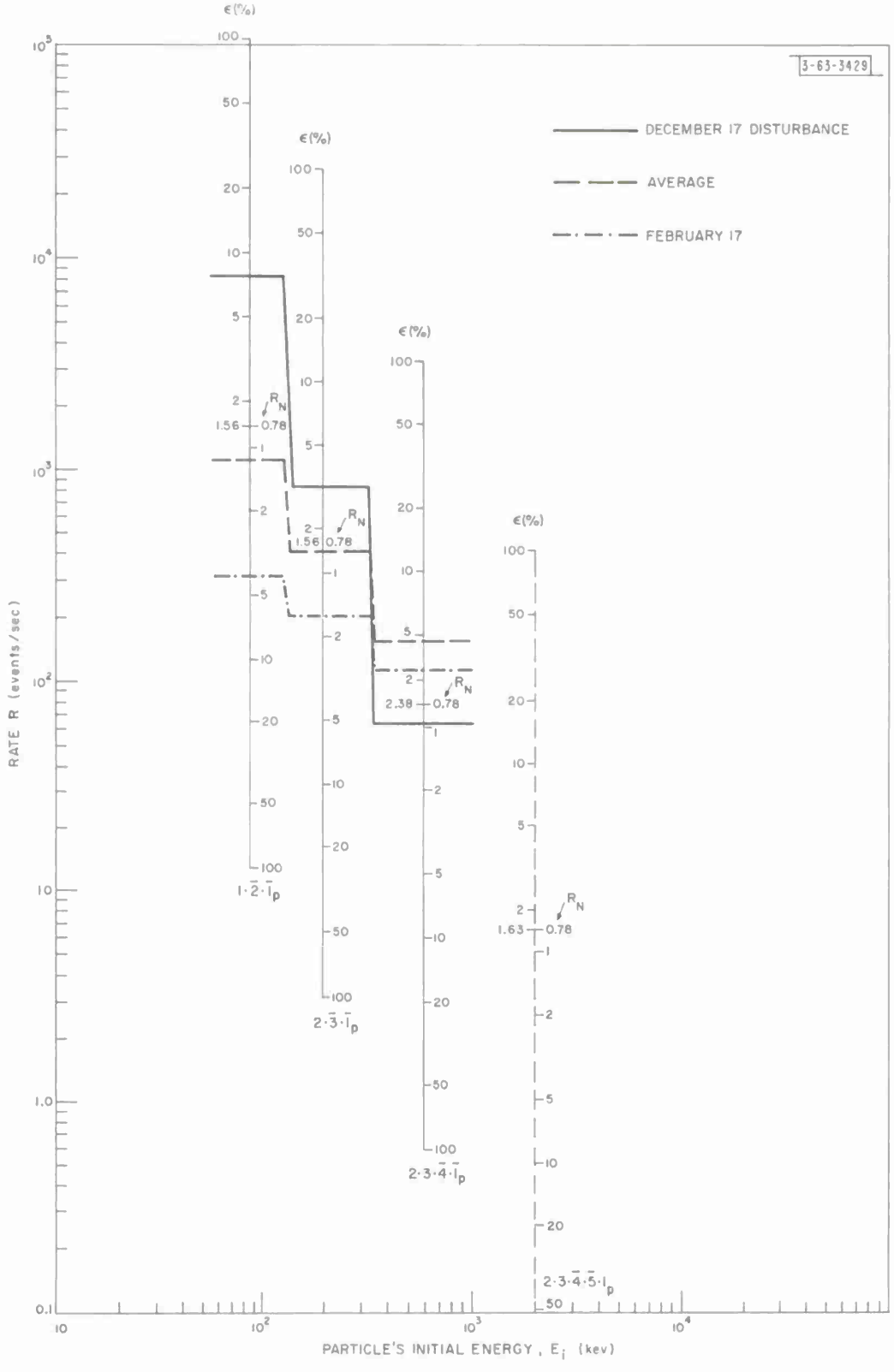

Fig. 14 Differential Measurements. Counting rate vs. particle's energy showing relative error at each rate and previously measured spectrum.

Finally, it must be pointed out that the degree of latitude and flexibility available in the design must not lure the experimenter into a false sense of security. The approach taken in this experiment is quite different from that reported by Frank, Van Allen and Hills. The amount of flux lost due to scattering in this experiment is feared to be significant and thus will lower the expected rates at the higher energies. This effect has been allowed for by this author, but only extensive and careful laboratory testing can insure that the proposed design herein will adequately span the uncertainties.

M_1: Differential Measurement $1 \cdot \overline{2} \cdot \overline{1_p}$

This measurement will be used to determine the flux (particles/cm^2 sec) of electrons which have energies within a differential band between 60 kev and 130 kev. The technique is to accept as legitimate counts only those particles which have the following properties simultaneously:

a) lose sufficient energy in detector #1 to produce a signal which triggers electron discriminator 1;

b). do not lose sufficient energy in detector #2 to produce a signal which triggers the electron discriminator 2;

c). do not lose sufficient energy in detector #1 to produce a signal which triggers the proton discriminator 1_p.

Energy Band: $60 \text{ kev} < E_e < 130 \text{ kev}$

Expected Nominal Rate*: $300 < R_N < 8000$ events/sec

*Ibid.

Choose $T_o = 1 \times .08 \text{ sec} = 0.08 \text{ sec}$

so that $R_N = 1600$ events/sec

(The gating times for each measurement is conveniently chosen in increments of .08 sec since this is the duration of a single telemetry word, and thus simplifies the timing and control logic).

For $K \geq \frac{6400}{R_N} = \frac{6400}{1600} = 4$ choose $K = 4 = 2^2$

Then $\epsilon_H\Big|_{min} = \frac{R_N}{4096} \times K = 1.56\%$

$$R_H\Big|_{\epsilon_H = 100\%} = \frac{409600}{4} = 102,400 \text{ events/sec}$$

M_2 : Differential Measurement $2.\overline{3}.\overline{I}_p$

Energy Band: 140 kev $< E_\epsilon <$ 330 kev

Expected Nominal Rate: $190 < R_N < 830$ events/sec

Choose $T_o = 4 \times .08 = 0.32$ sec

so that $R_N = 400$ events/sec

For $K \geq \frac{6400}{400} = 16$ choose $K = 16 = 2^4$

Then $\epsilon_H\Big|_{min} = 1.56\%$

$$R_H\Big|_{\epsilon_H = 100\%} = \frac{409600}{16} = 25,600 \text{ events/sec}$$

M_3 : Differential Measurement $2 \cdot 3 \cdot \overline{4} \cdot \overline{T}_p$

Energy Band: $350 \text{ kev} < E_\epsilon < 1 \text{ Mev}$

Expected Nominal Rate: $60 < R_N < 250$ events/sec

Choose $T_o = 21 \times .08 = 1.68$ sec

so that $R_N = 76$ events/sec in anticipation of a lowering of expected rates due to scattering, etc.

For $K \geq \frac{6400}{76} = 84$ choose $K = 128 = 2^7$

Instead of choosing $K = 2^7$ with $T_c = 2^{-5} \times 10^{-2}$ sec a more convenient arrangement is to use the lower clock frequency with $T'_c = 10^{-2}$ sec and thus use a $K' = 2^2$.

Then $\epsilon_H\Big|_{min} = \frac{76 \times 128}{4096} = 2.38\%$

and $R_H\Big|_{\epsilon_H = 100\%} = \frac{409600}{128} = 3200$ events/sec

M_4 : Differential Measurement $2 \cdot 3 \cdot 4 \cdot \overline{5} \cdot \overline{T}_p$

Energy Band: $1 \text{ Mev} < E_\epsilon <$ (see note below)

Expected Nominal Rate: (see note below)

Choose $T_o = 245 \times .08 = 19.6$ sec

so that $R_N = 6.5$ events/sec

For $K \geq \frac{6400}{6.5} = 980$ choose $K = 2^{10}$

or better choose $K' = 2^5$

Note: At the time of this writing the characteristics of the fifth detector and the absorber in front of it were unknown to this author. In the design of this measurement guestimates of the rates were made with allowances for decreases due to scattering, etc.

Then $\varepsilon_H\Big|_{min} = \frac{6.5 \times 1024}{4096} = 1.63\,\%$

$$R_H\Big|_{\varepsilon_H = 100\,\%} = \frac{409600}{1024} = 400 \text{ events/sec}$$

M_5 : Integral Measurement $2 \cdot 3 \cdot 4 \cdot \bar{I}_p$

Energy Range: $E_\epsilon > 1$ Mev

Expected Nominal Rate: $4 < R_N < 120$ events/sec

Choose $T_o = 63 \times .08 = 5.04$ sec

so that $R_N = 25.4$ events/sec

For $K \geq \frac{6400}{25.4} = 252$ choose $K = 2^8$

or better $K' = 2^3$

Then $\varepsilon_H\Big|_{min} = \frac{25.4 \times 256}{4096} = 1.59\,\%$

$$R_H\Big|_{\varepsilon_H = 100\,\%} = \frac{409600}{256} = 1600 \text{ events/sec}$$

M_6 : Integral Measurement $2 \cdot \bar{I}_p$

Energy Range: $E_\epsilon > 140$ kev

Expected Nominal Rate: $400 < R_N < 900$ events/sec

Choose $T_o = 2 \times .08 = 0.16$ sec

so that $R_N = 800$ events/sec

For $K \geq \frac{6400}{800} = 8$ choose $K = 2^3$

Then $\epsilon_H\Big|_{min} = 1.56\,\%$

$$R_H\Big|_{\epsilon_H = 100\,\%} = \frac{409600}{8} = 51,200 \text{ events/sec}$$

M_7 : Integral Measurement $2 \cdot 3 \cdot \bar{T}_p$

Energy Range: $E_\epsilon > 350$ kev

Expected Nominal Rate: $70 < R_N < 250$ events/sec

Choose $T_o = 8 \times .08 = 0.64$ sec

so that $R_N = 200$ events/sec

For $K \geq \frac{6400}{200} = 32$ choose $K = 2^5$

Then $\epsilon_H\Big|_{min} = \frac{200 \times 32}{4096} = 1.56\,\%$

$$R_H\Big|_{\epsilon_H = 100\,\%} = \frac{409600}{32} = 12,800 \text{ events/sec}$$

M_8 : Integral Measurement $2 \cdot 3 \cdot 4 \cdot 5 \cdot \bar{T}_p$

Energy Range: (see note for M_4)

Expected Nominal Rate: (see note for M_4)

Choose $T_o = 489 \times .08 = 39.12$ sec

so that $R_N = 3.28$ events/sec

For $K \geq \frac{6400}{3.28} = 1950$ choose $K = 2^{11}$

or better $K' = 2^6$

Then $\epsilon_H\Big|_{min} = \frac{3.28 \times 2048}{4096} = 1.64\%$

$$R_H\Big|_{\epsilon_H = 100\%} = \frac{409600}{2048} = 200 \text{ events/sec}$$

M_s : Source Calibration

It is desirable to monitor the effects of the satellite's environment upon a detector. To this end, a separate detector and measurement chain will be included. The detector will be exposed to a known source of radiation and will count directly the decay particles.

At the time of this writing neither the type and strength of the source, nor the characteristics of the detector have been specified. However, the following design parameters are proposed.

Choose $T_o = 90 \times .08 = 7.20$ sec

so that $R_N = 17.8$ events/sec

For $K \geq \frac{6400}{17.8} = 360$ choose $K = 2^9$

or better $K' = 2^4$

TABLE II

SUMMARY OF DESIGN PARAMETERS

Measurement	Designation	Duration (sec)	No. of Telemetry Words	Clock Divider K or K'	Telemetry Clock
$1 \cdot \overline{2} \cdot \overline{1}_p$	M_1	0.08	1	2^2	32 fc
$2 \cdot \overline{3} \cdot \overline{1}_p$	M_2	0.32	4	2^4	32 fc
$2 \cdot 3 \cdot \overline{4} \cdot \overline{1}_p$	M_3	1.68	21	2^2	fc
$2 \cdot 3 \cdot 4 \cdot \overline{5} \cdot \overline{1}_p$	M_4	19.6	245	2^5	fc
$2 \cdot 3 \cdot 4 \cdot \overline{1}_p$	M_5	5.04	63	2^3	fc
$2 \cdot \overline{1}_p$	M_6	0.16	2	2^3	32 fc
$2 \cdot 3 \cdot \overline{1}_p$	M_7	0.64	8	2^5	32 fc
Calibration Source	M_s	7.20	90	2^4	fc
$2 \cdot 3 \cdot 4 \cdot 5 \cdot \overline{1}_p$	M_8	39.12	489	2^6	fc

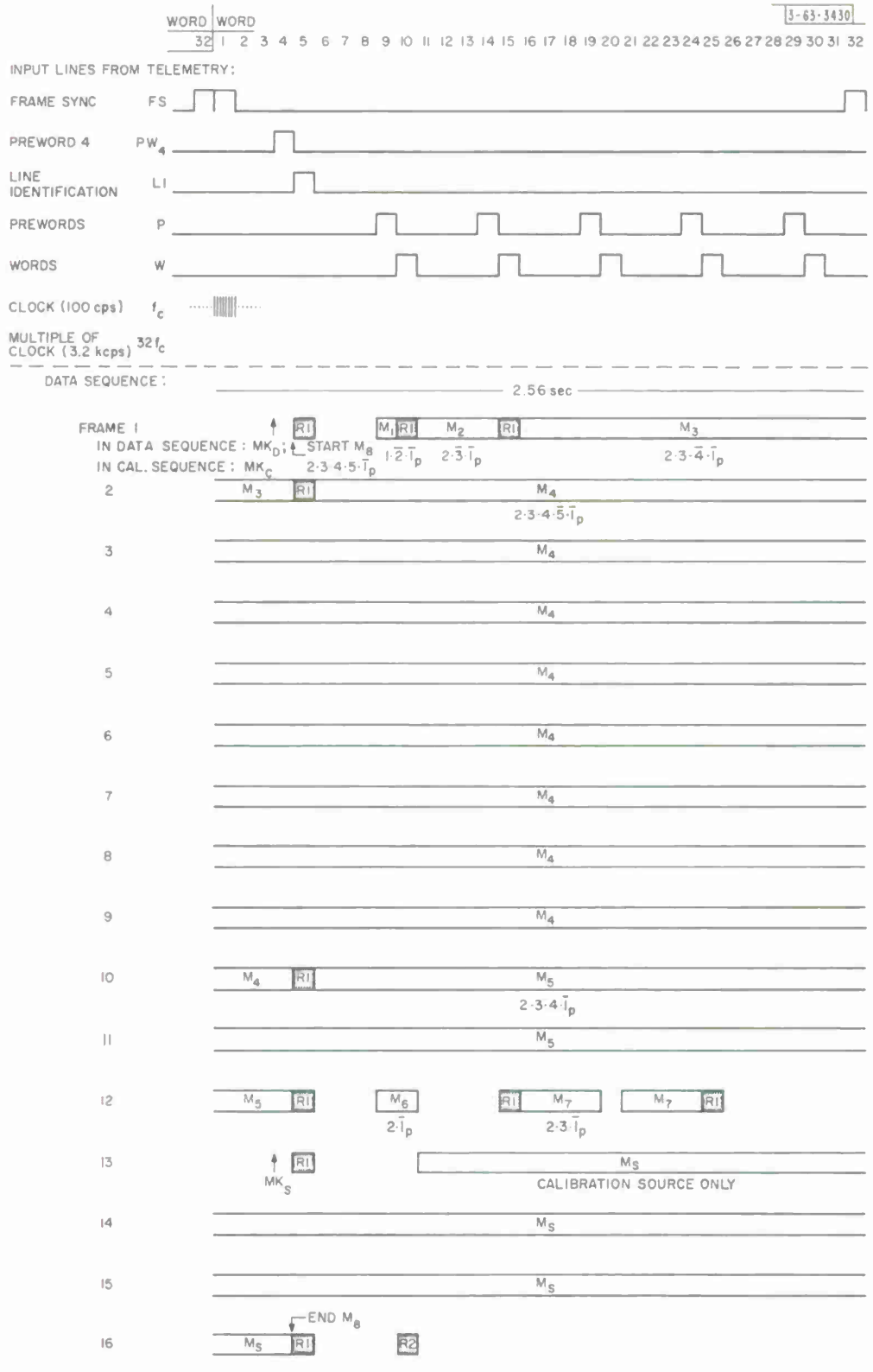

Fig. 15 Telemetry Format

Then $\epsilon_H\Big|_{min} = 2.23\,\%$

$$R_H\Big|_{\epsilon_H = 100\,\%} = 800 \quad \text{events/sec}$$

D. The Data Sequence

The previous discussion of the Hybrid Counter resulted in the required duration of each measurement, as well as the parameters K and clock frequency. The arrangement of these data gathering periods into a single data sequence will now be outlined (see Fig. 15).

The telemetry package makes available seven lines (illustrated on the top of Fig. 15) to the experiment. It is noted that a frame of telemetry contains 32 words, and is 2.56 sec long. Thus 16 frames will comprise a sequence (40.96 sec). There are six readout words per frame available to this experiment: word #5 (on a separate line, called LI) and words 10, 15, 20, 25 and 30 (on the word line, called W). Other lines are as indicated.

Each sequence is begun by loading into Hybrid Counter #1, a unique word, easily recognizable as a marker word. If the sequence is a data sequence then the marker word is 11111111; for a calibration sequence it is 00110011. These words will never occur in practice since the Hybrid Counter automatically is prevented from counting past the word 00000011.

Having loaded Hybrid Counter #1 with this unique word, it is immediately read out to the telemetry system during the first readout word of frame 1 (F_1), which is the line identification word (LI).

The first differential measurement, M_1 $(1 \cdot \overline{2} \cdot \overline{T}_p)$, is now undertaken for a period of time equal to one telemetry word. This is conveniently the first word on the P line, (called P_1) during frame 1 (F_1). Hybrid Counter #1 is then read out during the next available readout time which is the first word on the W line (W_1) of F_1.

The second differential measurement, M_2 $(2 \cdot \overline{3} \cdot \overline{T}_p)$, is next undertaken for a period of time equal to four telemetry words. This is conveniently done from the trailing edge of W_1, call it $TE(W_1)$, to the trailing edge of P_2 call it $TE(P_2)$ both in frame 1. The contents of Hybrid Counter #1 are read out during W_2 of this frame.

The sequence proceeds as indicated in Fig. 15 until the end of frame 12 (F_{12}). At this time all four differential measurements, and three integral measurements have been made by time sharing Hybrid Counter #1. In the time remaining of the sequence, Hybrid Counters #1 is used to monitor the source detector. The start of the source monitoring is indicated by the marker word 00001111.

The fourth integral measurement (M_8) is accomplished by accumulating data in a separate Hybrid Counter #2. This measurement is performed during the same time as the others and begins early in frame 1 ($TE(PW_4)$) and ends during frame 16 ($TE(PW_4)$). The contents of Hybrid Counter #2 are then read out during the first W word of frame 16.

The calibration sequence has the exact same arrangement of measurements, only the detectors are electrically disconnected from the experiment (by disabling their bias voltages) and simultaneous test signals are applied to all measurement chains.

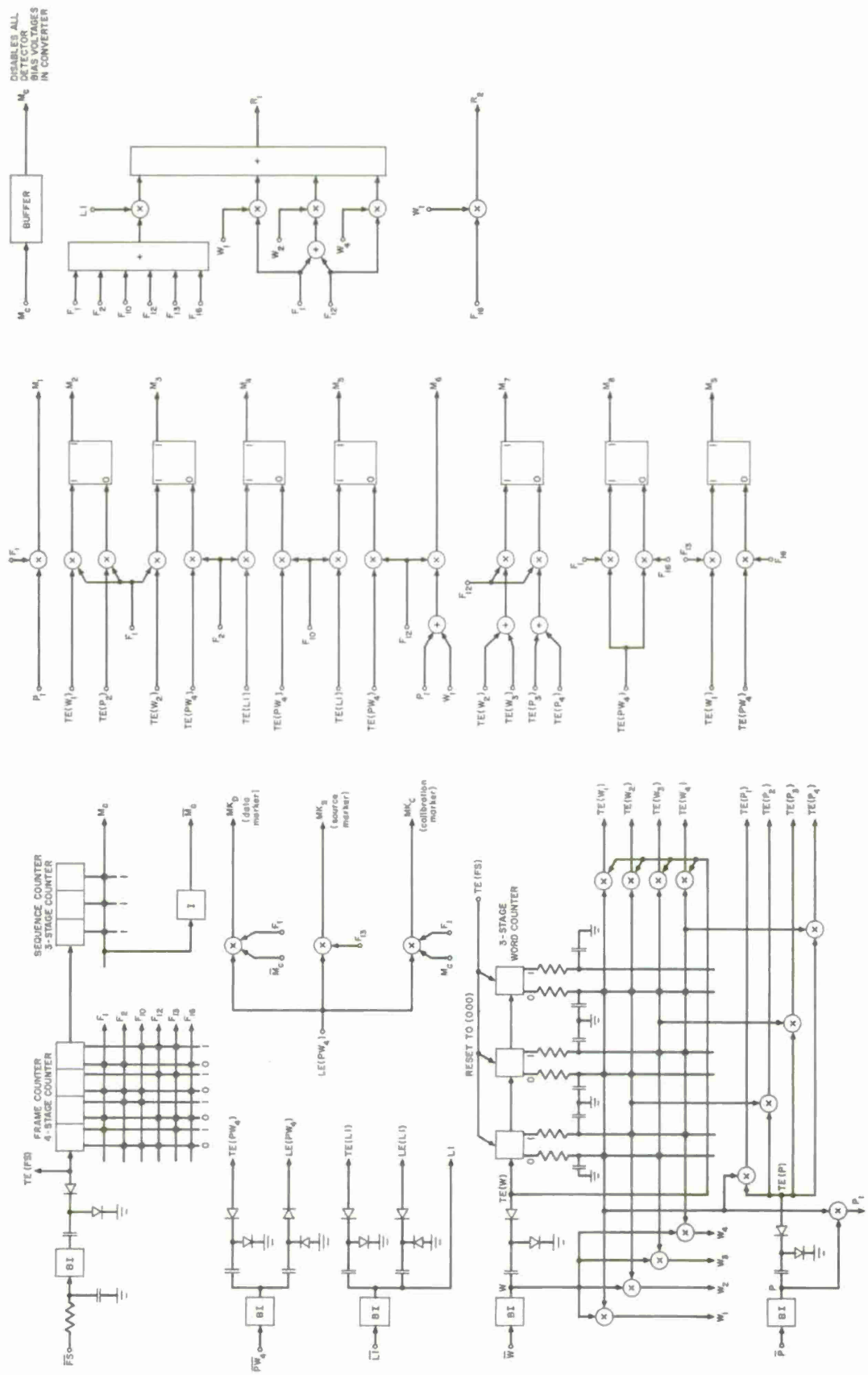

Fig. 16 Timing and Control Logic Block Diagram

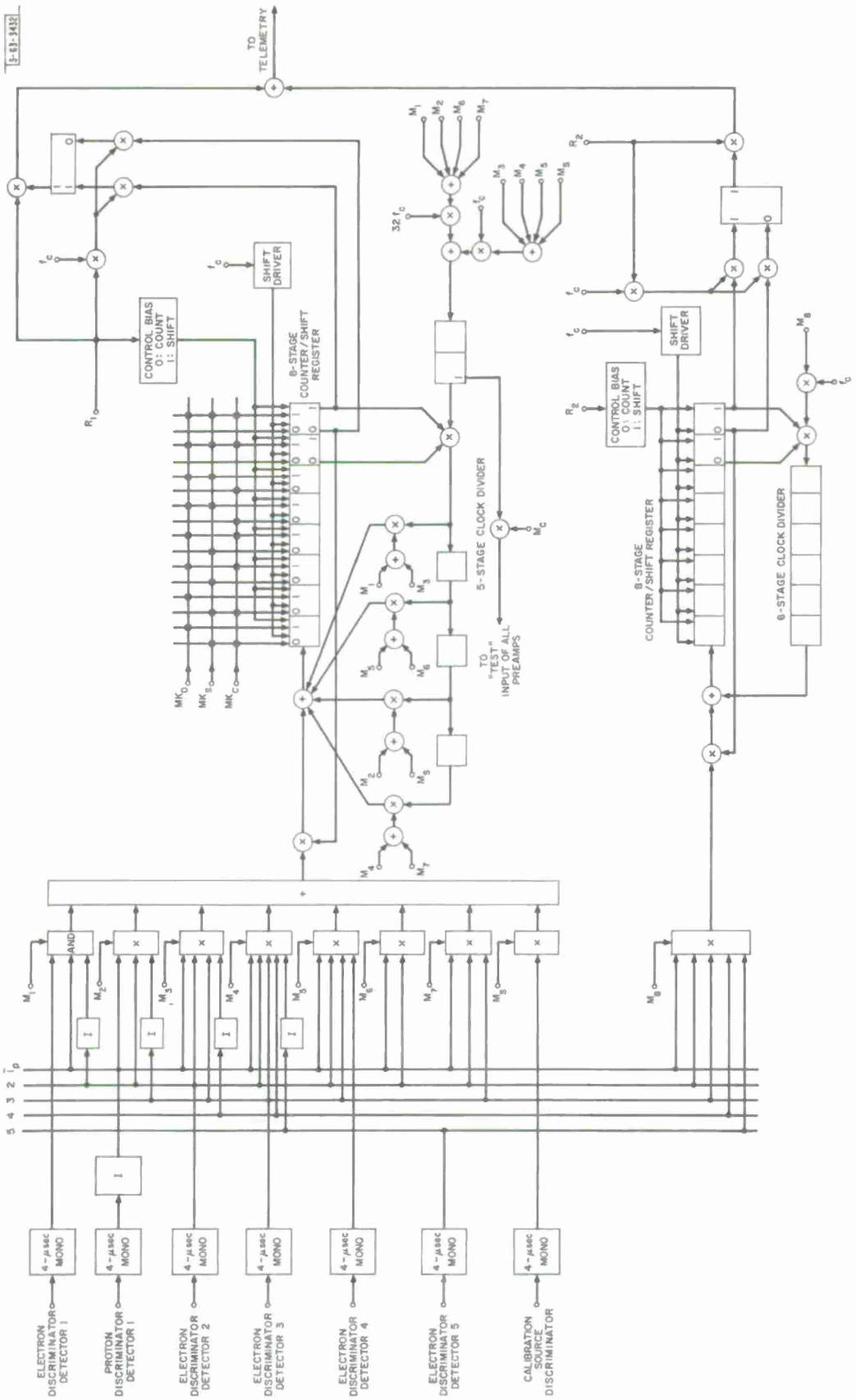

Fig. 17 Coincidence and Counter Logic Block Diagram

E. The Logical Design

To accomplish the desired measurements in the order indicated, the necessary Timing and Control Logic, Fig. 16 was developed. In this diagram can be found the frame counter, the sequence counter, the word counter, various strobe pulse formed from the leading or trailing edges of key words, the three marker strobes, the eight measurement gates, the source gate and the calibration sequence level. The readout times for Hybrid Counter #1 and #2 are designated R_1 and R_2, respectively.

The timing and control signals developed are used to control the operation of the Coincidence and Counter Logic, Fig. 17. Here can be found the waveform stabilizing monostables triggered by the discriminators, the coincidence logic to form the required inputs to the Hybrid Counters #1 and #2, the strobed marker words, the readout logic and the clock derived test signals used during the calibration sequence.

These two diagrams represent the culmination of the foregoing analysis of the experiment for the output of the detectors to the input to the telemetry system. The design of the measurement chain and discriminator will now be discussed in further detail in the following section.

IV. THE MEASUREMENT CHAIN

A. General

The purpose of the measurement chain of the radiation experiment is to linearly produce a signal from the charge liberated in a detector by the loss of energy of an incident particle. The signal is usually in the form of a voltage developed across a capacitor by the collection of either the ion or electron charge carriers.

The measurement chain consists of a preamplifier, a filter, and a post amplifier. The following is a discussion of some of the considerations that were involved in arriving at the present design.

B. The Detector's Output

A solid state detector is basically a very dense ionization chamber. The incident particle loses energy through ionization* as it passes through the depletion region in the back biased diode. The energy lost per ion-electron pair is roughly 3.5 ev/ion-el. pair. The time required for the charges to appear at the detector's terminals is

$$t = \frac{d}{v} = \frac{d}{\mu E} = \frac{d^2}{V\mu}$$

Example $\mu_e = 1500 \frac{cm^2}{volt\text{-}sec}$ for electrons

$d = 500$ microns

$V = 140$ volts

Then $t \approx 10$ nanosec max.

Thus for all practical purposes the charge can be considered to be collected instantaneously (an impulse of current), and the voltage developed across the detector's capacitance can be represented as a voltage step due to this impulse of current. The equivalent circuit can then be developed in either of two equivalent ways.

---

* This, of course, is not the only means of energy loss, but it is the one of interest in this analysis.

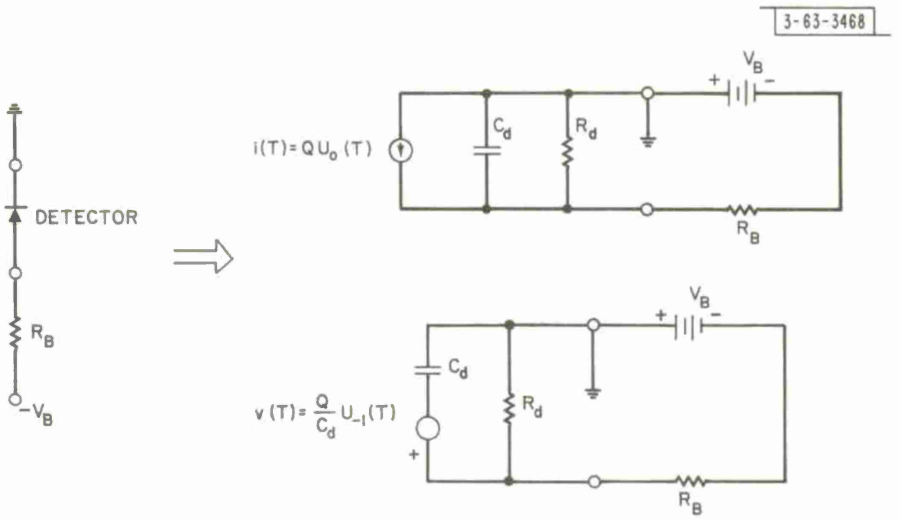

C. The Preamplifier

The oldest type of feedback stabilized preamplifier is the voltage-sensitive type, where the output voltage is simply a multiple of the input voltage developed across the detector.

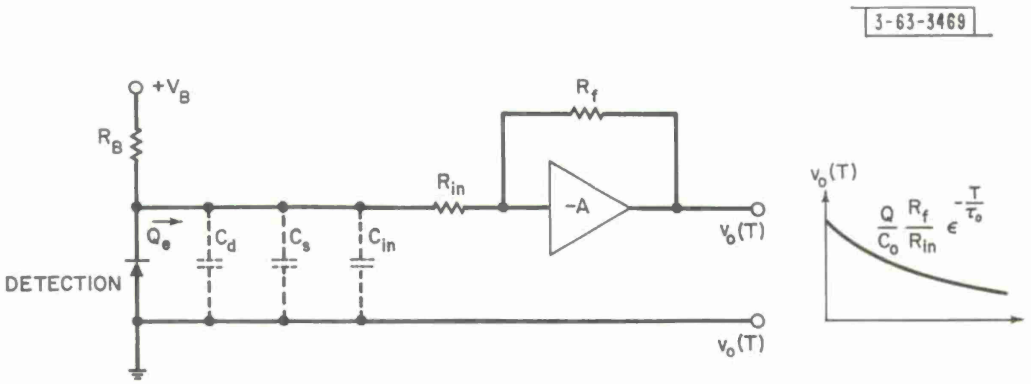

$$C_o = C_{detector} + C_{stray} + C_{input}$$

$$R_o = R_B // R_{in}$$

$$\tau_o = R_o C_o$$

Voltage Sensitive Preamplifier Configuration

(illustrating method of electron charge collection with negative input voltage to the preamplifier).

The principal shortcoming of the voltage-sensitive preamplifier is its sensitivity to changes in the capacities which constitute C_o. This was unimportant until the introduction of the solid state detector whose capacity can change appreciably with environment and circuit conditions.

In the charge-sensitive preamplifier, the detector, stray and input capacities are degenerated, and nearly all of the liberated charge appears on the feedback capacitor, C_f, which can be of the zero temperature coefficient variety for good stability.

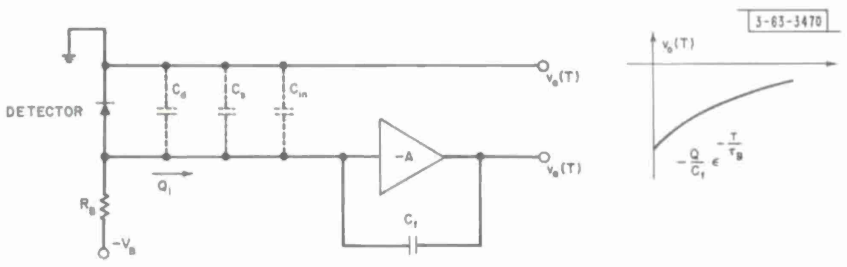

$$C_o = C_d + C_s + C_{in}$$

$$\tau_B \approx R_B C_o$$

Charge Sensitive Preamplifier

(illustrating the method of ion charge collection with positive input voltage to the preamplifier)

In the analysis of the preamplifier the following model is used:

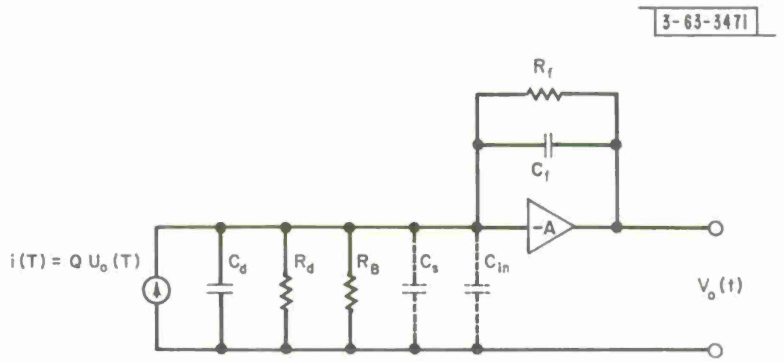

Using the standard feedback analysis, this model reduces to:

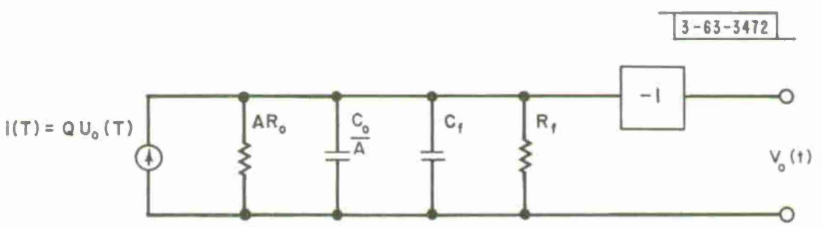

where $R_o = R_d /\!/ R_B$

$$C_o = C_d + C_s + C_{in}$$

This configuration places in evidence:

1. The degeneration of the detector, stray and input capacity, and the dominance of the feedback capacitor in the role of charge collection.

2. The output time constant is predominately governed by the feedback time constant $\tau_f = R_f C_f$. The three conditions for these observations to hold are:

1. $A \gg 1$
2. $\frac{C_o}{A} \ll C_f$
3. $AR_o \gg R_f$

Normally, insuring the first condition through use of a high gain amplifier, is sufficient. A high gain amplifier is also desirable since its use degenerates the effect of changes in C_o upon the output voltage

$$\frac{dv_{out}}{v_{out}} = \frac{1}{A} \frac{C_o}{C_f} \left(\frac{dC_o}{C_o} \right)$$

One should attempt to minimize C_o in whatever way possible for three reasons:

1. To make the output voltage independent of its value
2. To make the output voltage insensitive to changes in its value
3. To reduce the effective input noise. This point will be discussed further in the next section.

The detector's capacity, C_d, is normally set by system considerations

such as particle collecting area and desired depletion layer thickness, and one usually has to live with this capacitance as given.

Stray capacity, C_s, can be reduced by layout, lead length, and mounting considerations. The use of shielded wire from the detector to the preamp, while reducing stray pickup, increases C_s so that other means of coupling or placement of the detector and preamp should be explored.

The effective input capacity of the preamp, C_{in}, can best be reduced by avoiding the regenerative Miller effect of a normal high gain amplifier. This is accomplished by employing a cascode front end which holds the input capacity to its "cold" value of $C_{cb} + C_{bE}$.

In the preamplifier studied, Fig. 18, the cascode stage employs a low noise high gain NPN(2N3117) to drive the grounded base PNP. Positive feedback (bootstrap) is applied from the output emitter follower back to the split collector load to increase the open loop gain near the frequencies of interest. A NPN/PNP cascode is used in preference to a pure NPN/NPN to permit the output d. c. potential to be approximately the same as that of the input, and thus enables adequate d. c. feedback for temperature stabilization.

The operating point of the 2N3117 is chosen so that $I_c \approx 60\ \mu a$ and $V_{CE} \approx 4$ volts. It has been found that this condition best satisfies the conflicting requirements of low noise and adequate frequency response (both noise and gain bandwidth decreases with collector current). The open loop characteristics of the preamp are shown in Fig. 19.

A test signal can be applied to this preamp by the application of a positive voltage step to the small (2pf) capacitor. This will deposit a known

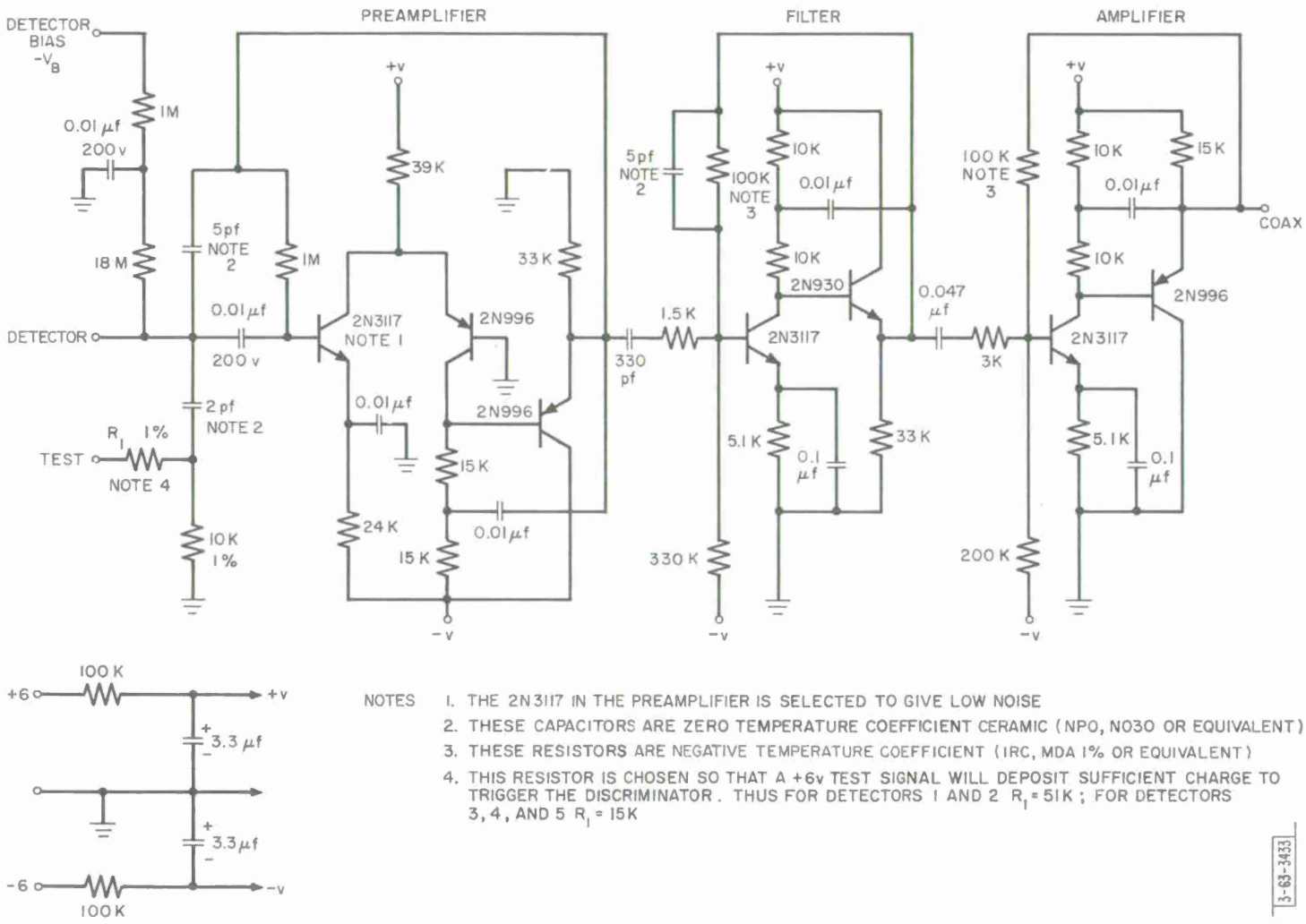

NOTES
1. THE 2N3117 IN THE PREAMPLIFIER IS SELECTED TO GIVE LOW NOISE
2. THESE CAPACITORS ARE ZERO TEMPERATURE COEFFICIENT CERAMIC (NPO, N030 OR EQUIVALENT)
3. THESE RESISTORS ARE NEGATIVE TEMPERATURE COEFFICIENT (IRC, MDA 1% OR EQUIVALENT)
4. THIS RESISTOR IS CHOSEN SO THAT A +6v TEST SIGNAL WILL DEPOSIT SUFFICIENT CHARGE TO TRIGGER THE DISCRIMINATOR. THUS FOR DETECTORS 1 AND 2 $R_1 = 51K$; FOR DETECTORS 3, 4, AND 5 $R_1 = 15K$

3-63-3433

Fig. 18 Measurement Chain

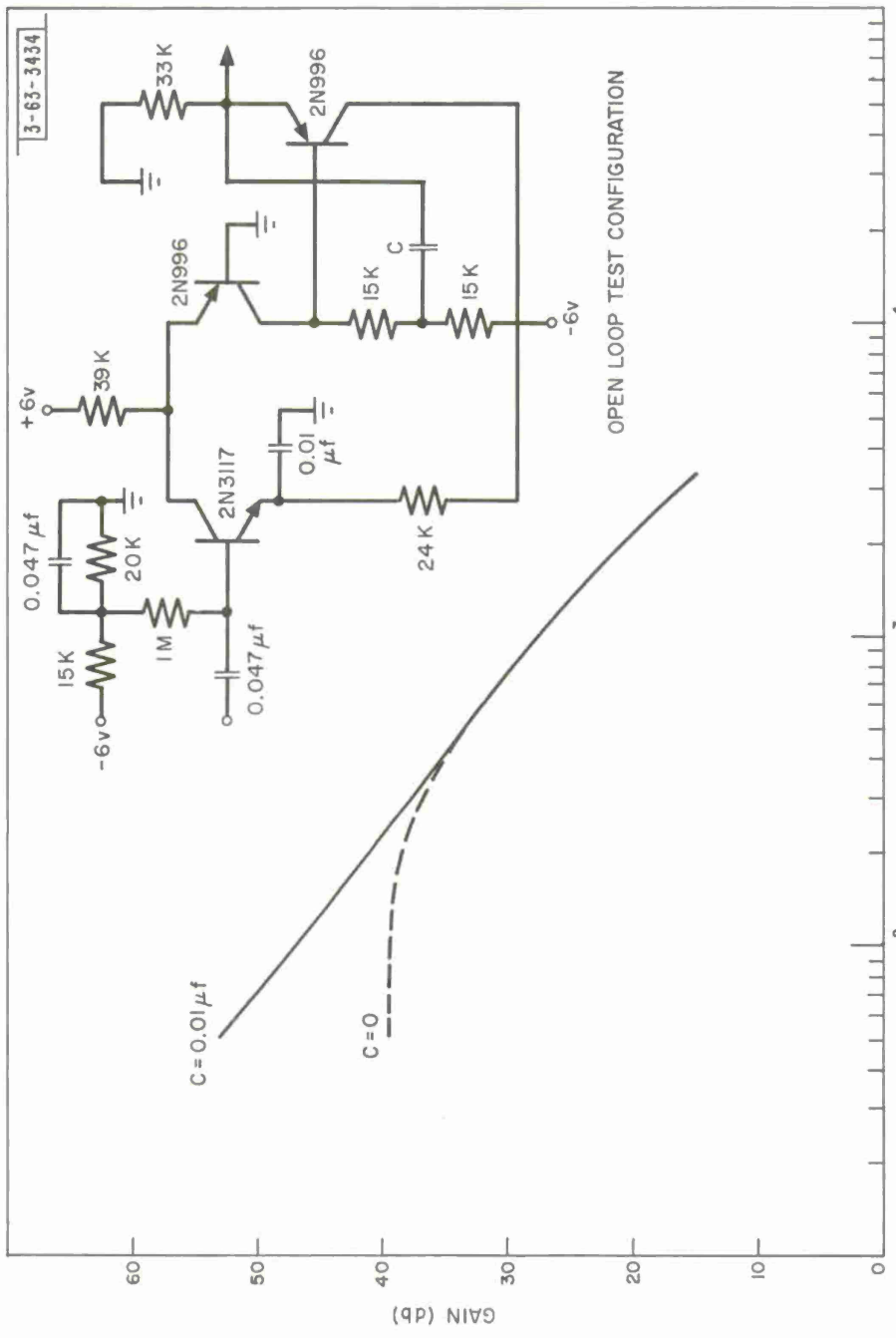

Fig. 19 Preamplifier Frequency Response

amount of charge at the input, similar to the charge liberated by an energetic particle passing through the detector. This feature is useful for laboratory testing of the preamplifiers and will also be used for in-flight calibration of the measurement chain, coincidence logic and hybrid counters by the application of voltage steps at an appropriate clock frequency to all preamps simultaneously.

The preamplifier draws 0.9 mw from +6 volts and 1.5 mw from -6 volts.

1. Preamplifier Noise:

Emmer* gives a fairly good account of the sources of noise to be expected in a transistor preamplifier for solid state detectors. He states that "any increase in C_o always results in a deacreased signal-to-noise ratio" but fails to prove this. Since this point is fairly important the following analysis shows the dependence of the noise line width on C_o in the case of white Gaussian noise. The detector equivalent circuit shown below is used.

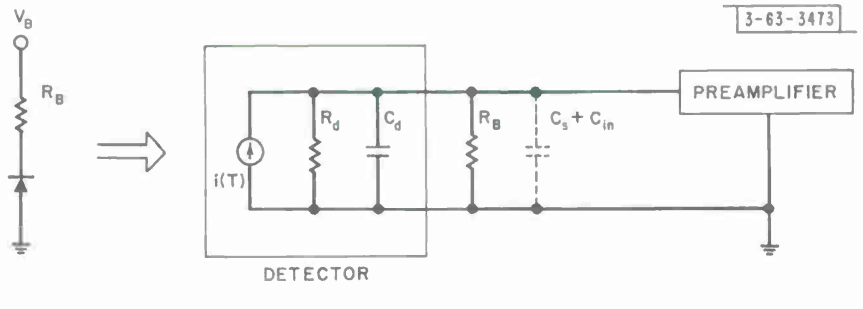

* T. L. Emmer, "Low Noise Transistor Amplifiers for Solid State Detectors", IRE Trans. Nuc. Sci., NS-8, No. 1, January 1961.

The fluctuating voltage at the input to the preamp is given by the expression

$$\overline{V^2}(f)\ df = 4kT\,R\ df$$

where $\overline{V^2}(f)\ df$ is the mean squared noise voltage of thermal origin in a bandwidth df

$R = R_d /\!/ R_B$

$C_o = C_d + C_s + C_{in}$

T = absolute temperature (^oK)

k = Boltzmann's constant

This white noise that is generated is limited to an upper frequency by the filtering action of R and C_o. The integrated mean squared noise voltage is then

$$\overline{V^2} = \int_o^\infty \frac{\overline{V^2}(f)\ df}{1 + \omega^2 C_o^2 R^2} = \int_o^\infty \frac{4kT\,R\ df}{1 + \omega^2 C_o^2 R^2}$$

giving $V_{noise}(rms) = \sqrt{\frac{kT}{C}}$ volts

The equivalent line width fwhm is then

$$E\ (\text{fwhm}) = \frac{3.5}{q}\ C\ V(\text{rms}) \times 2.35 \left(\frac{\text{fwhm}}{\text{rms}}\right),\ \text{Mev}$$

$$= 0.19 \sqrt{TC}\ \text{Kev}$$

where T is in ^{o}K

C is in pf

It is seen that the magnitude of the thermal noise contribution to counter resolution depends on C and not on R. In actual practice, the value obtained here is pessimistic, due to a required modification in the assumption of white Gaussian noise.

D. The Filter

In order to optimize the signal-to-noise ratio, the bandwidth of the measurement chain is limited to as narrow as possible consistent with permitted signal distortion requirements. For this purpose, a bandpass filter is inserted in the measurement chain.

It has been a stated requirement that the experiment be capable of processing events which may occur as rapidly as once every 10 μ sec. Thus the output must be restored to steady state conditions within 10 μ sec after an event.

The simplest narrow band filter is a single integrating and differentiating circuit with equal RC time constants. Equal time constants of 0.5 μ sec have been chosen to insure that the output is within 5 % of the peak after the 10 μ sec, bearing in mind the fact that all circuits are A.C. coupled and thus the undershoot following a pulse is the determining factor.

The filter used is shown in Fig. 18 and is basically an operational amplifier with the integrating and clipping parameters determined by the feedback and input circuit elements as shown below

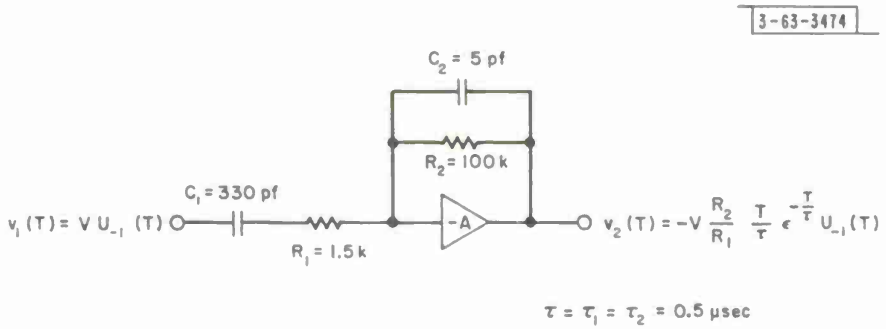

The high gain operational amplifier is patterned after the one used in the preamplifier. Here, however, a cascode front end is not necessary. The output emitter follower is directed to preferentially drive positive output pulses. The frequency response is shown in Fig. 20. The filter draws 1.2 mw from +6 volts and 0.1 mw from -6 volts.

E. The Post Amplifier

The post amplifier merely raises the signal to a level conveniently handled by the discriminator. It, too, is an operational amplifier whose input element has a large d.c. blocking capacitor to isolate the post amplifier and the filter. In the frequency range of interest the capacitor is a short circuit.

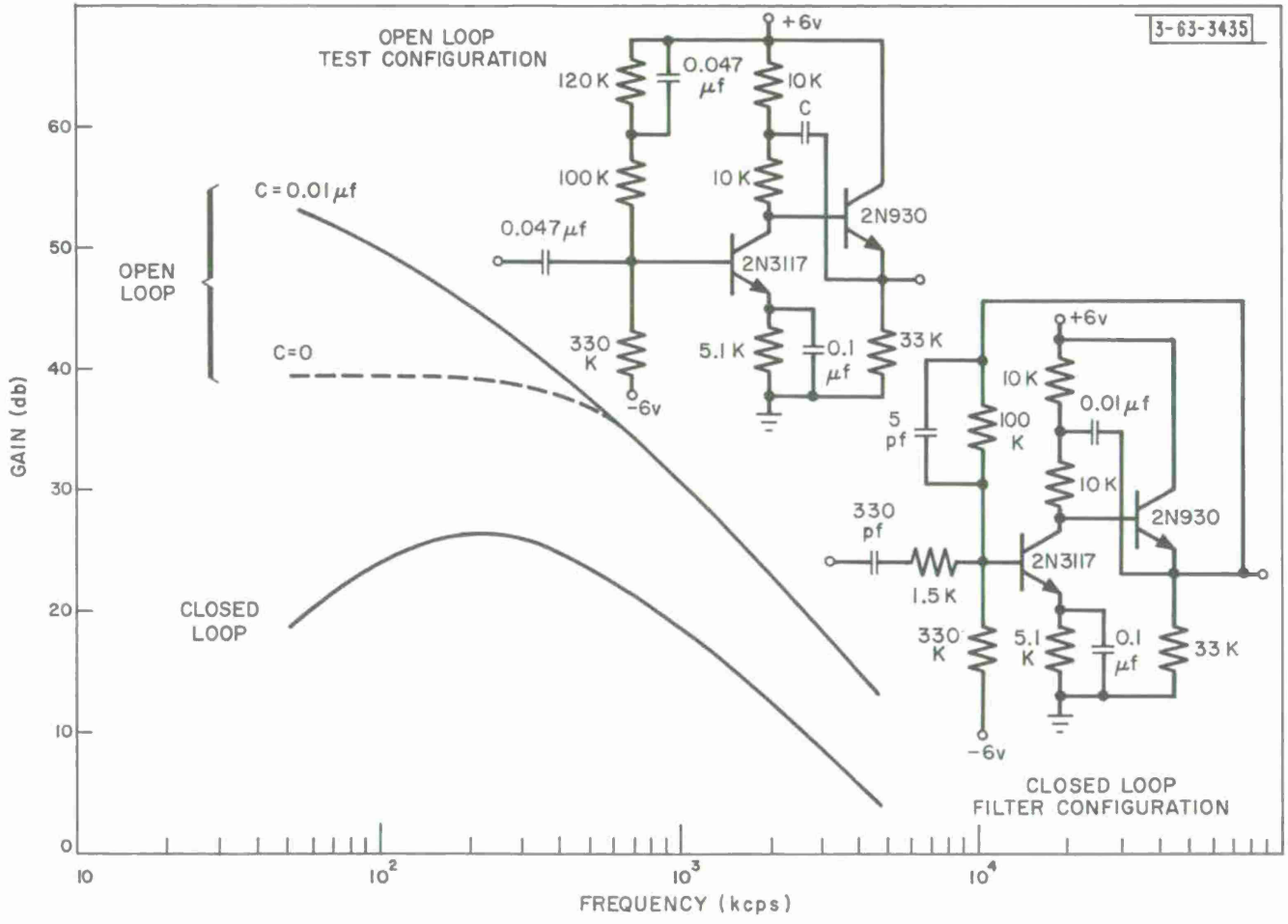

Fig. 20 Filter Frequency Response

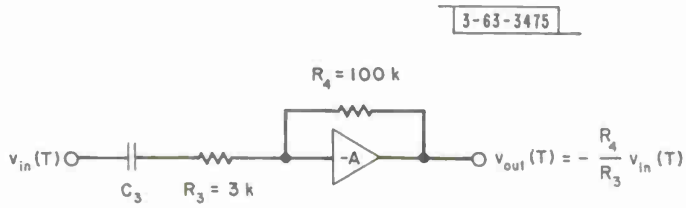

The pertinent frequency response curves are presented in Fig. 21. The response of the filter-post amplifier conbination is shown in Fig. 22. Here it should be noted that the differentiation is a pure RC while the integration is slightly steeper than a simple RC.

The post amplifier draws 1.2 mw from +6 volts, and 0.2 mw from -6 volts.

F. Testing the Measurement Chain

The measurement chain has been tested with various simulated detector capacities at different temperatures. Measurements of noise linewidth were made with a pulse height analyzer, which yields the best measurement of the true equivalent noise. The noise linewidth (full width half maximum in kev) is depicted in Fig. 23 and Fig. 24 with temperature and equivalent detector capacity as parameters. Detailed plots of the actual pulse height spectrums and photographs of the spectrum are shown in Figs. 25 through 35.

Figure 23 illustrates the dependence of the chain's conversion gain on temperature. Since the operating temperature of the chain is expected to be $0^{\circ}C$ plus or minus $15^{\circ}C$, the temperature dependence was designed to be convex about the nominal operating temperature.

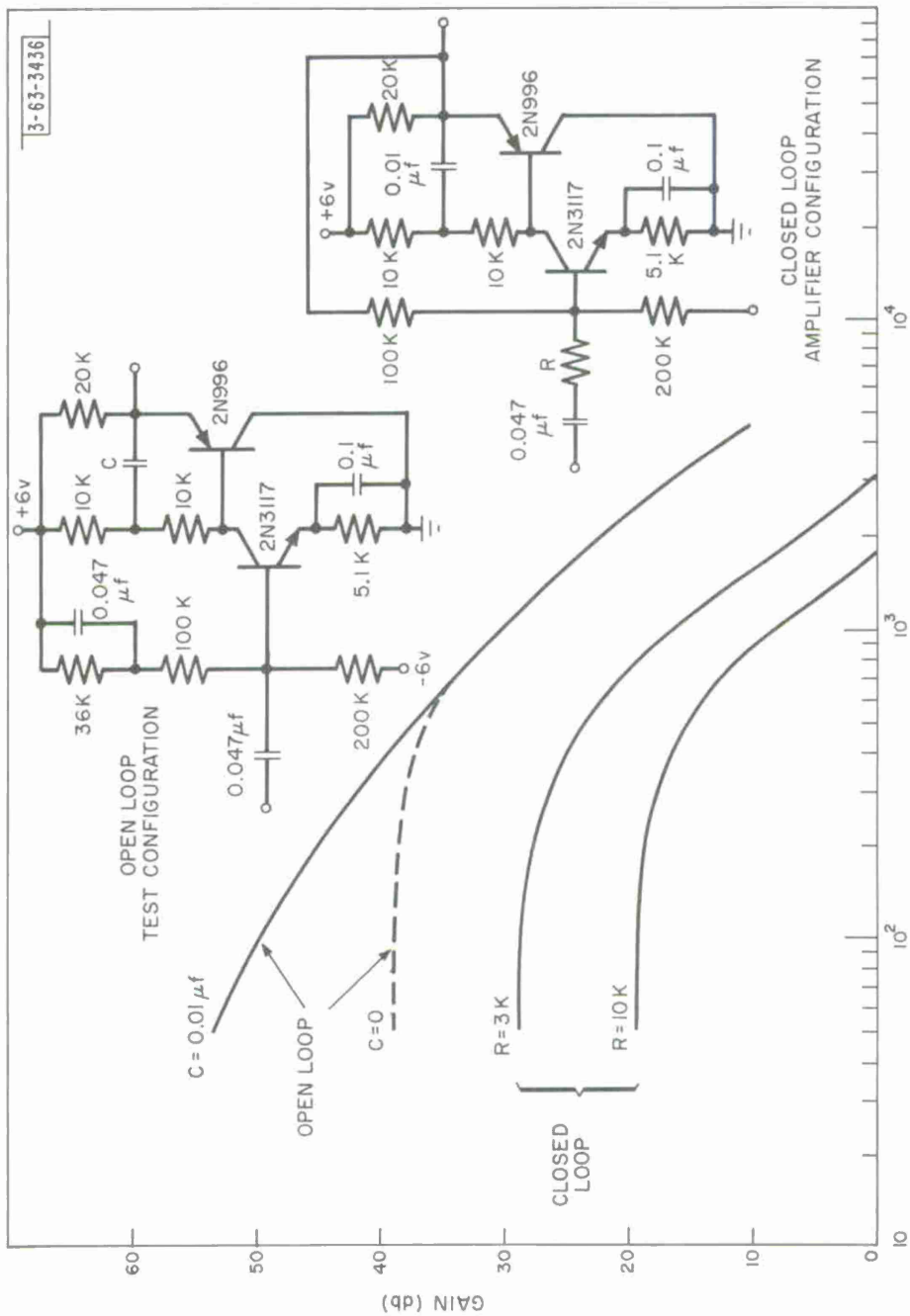

Fig. 21 Amplifier Frequency Response

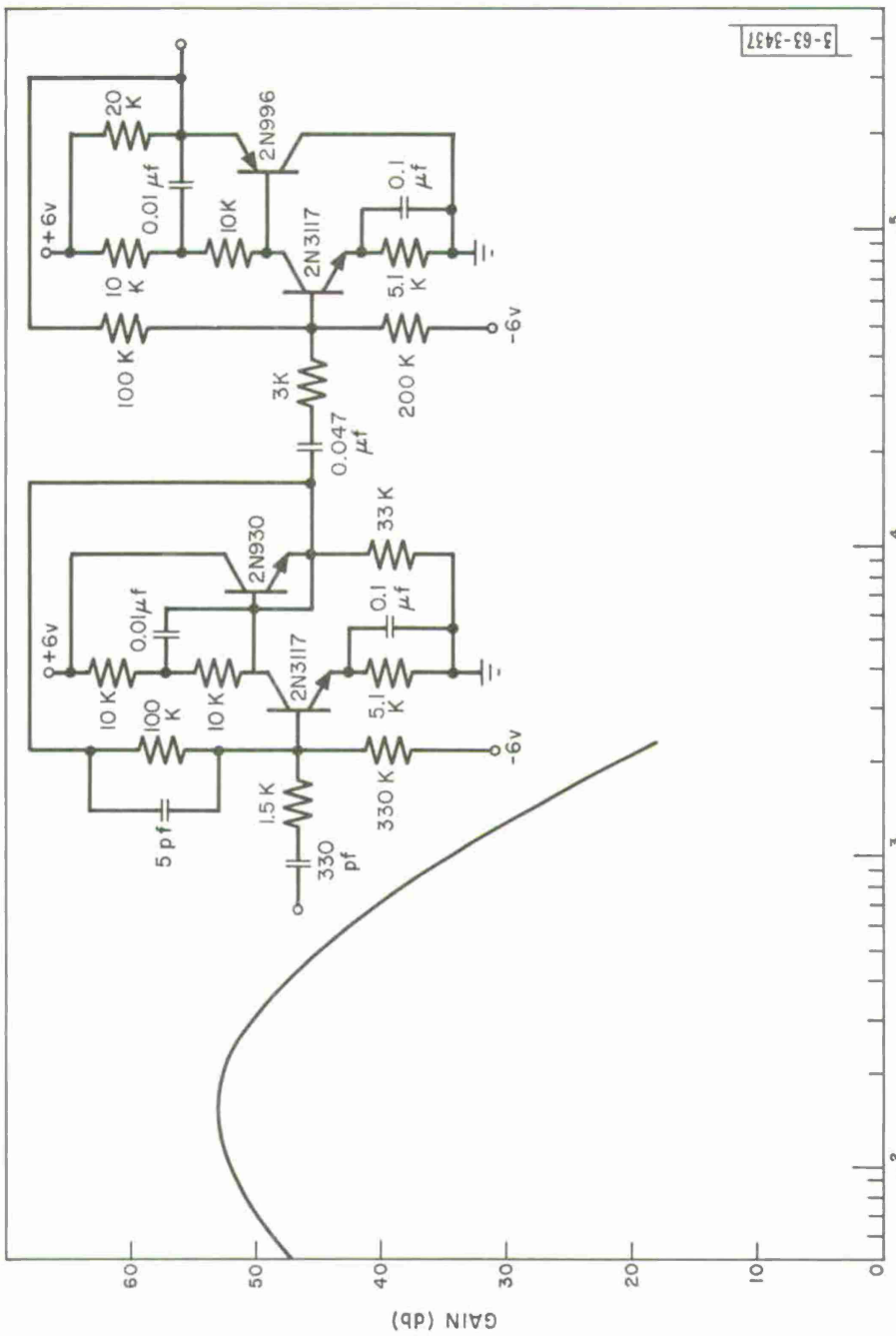

Fig. 22 Combined Filter and Amplifier Frequency Response

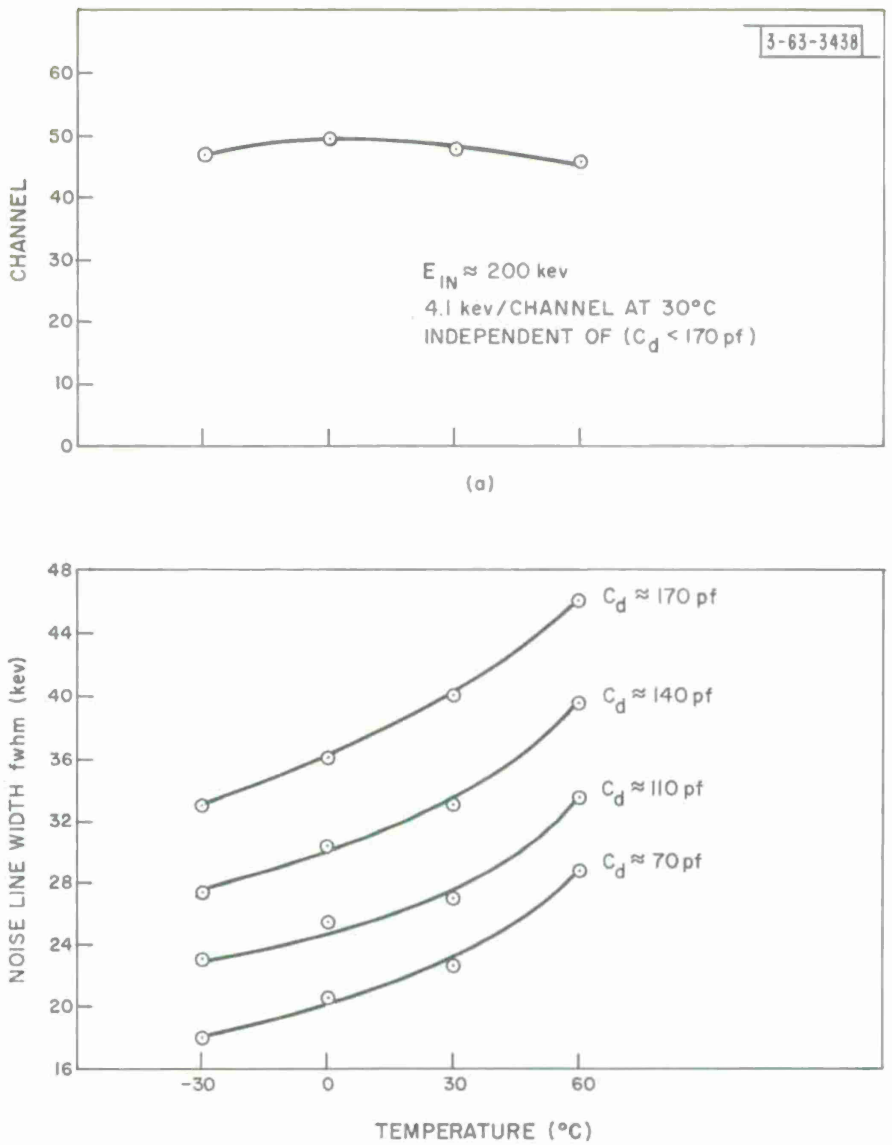

Fig. 23 Peak of Pulse Height Spectrum

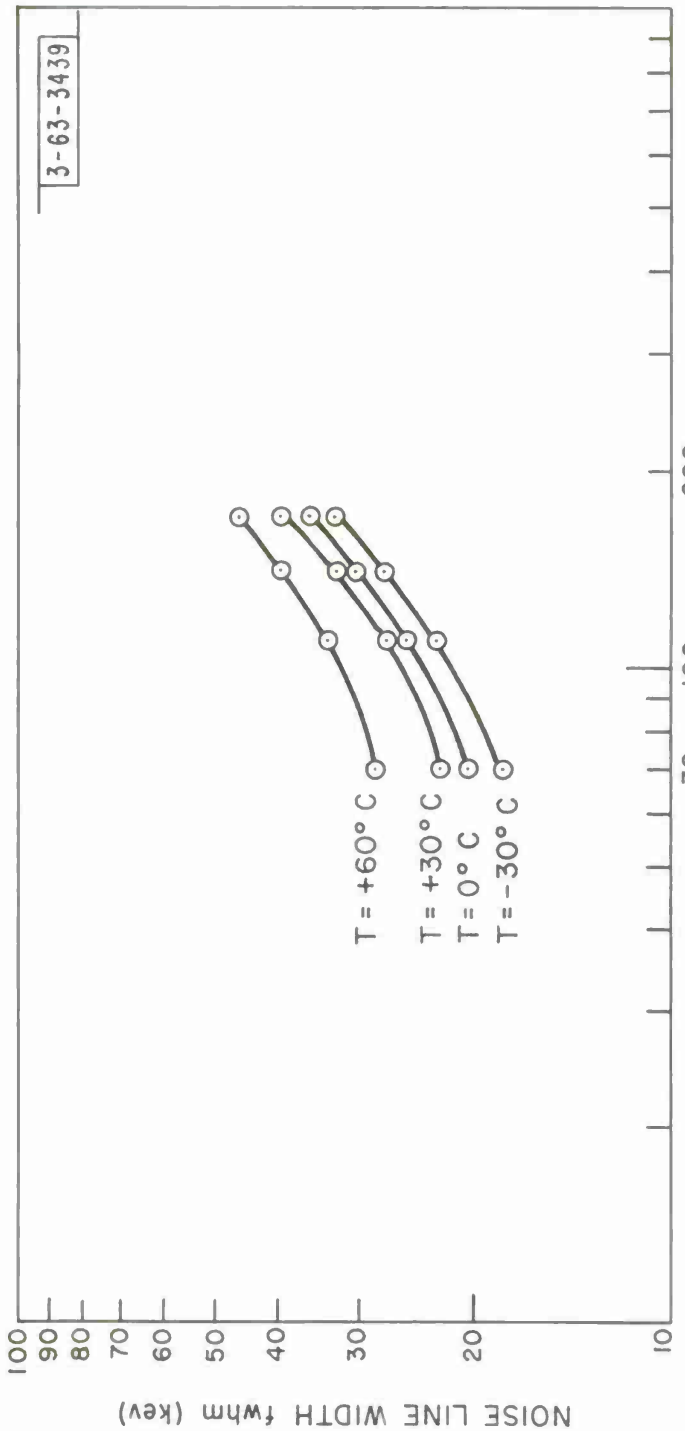

Fig. 24 Noise Line Width

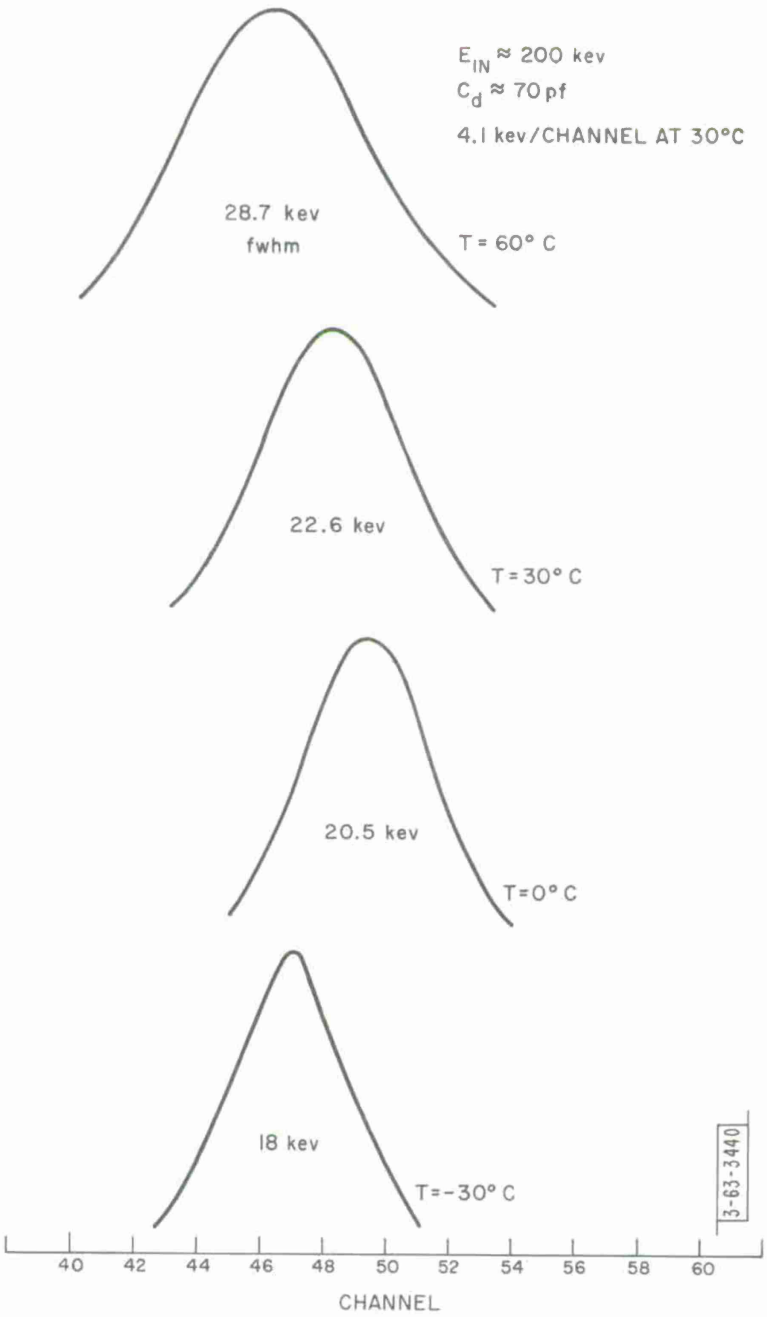

Fig. 25 Preamplifier Pulse Height Spectrum

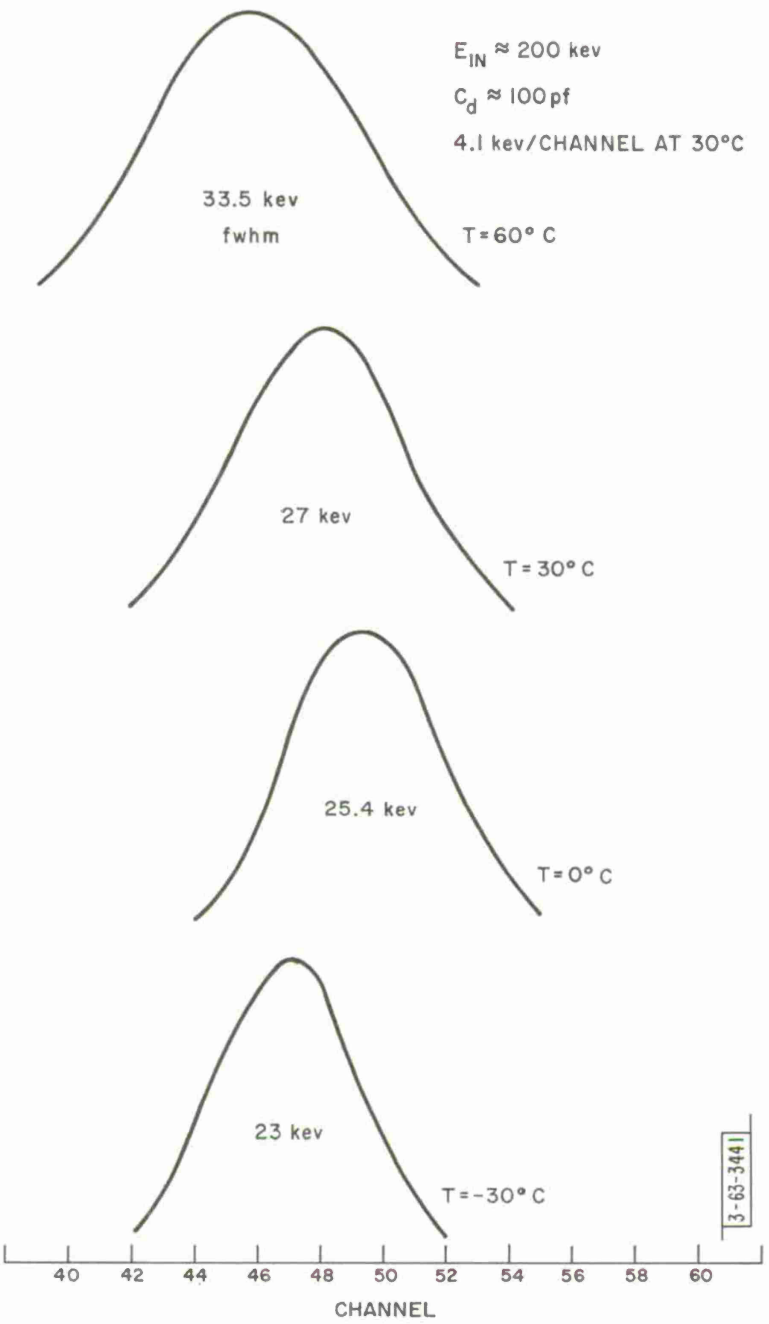

Fig. 26 Preamplifier Pulse Height Spectrum

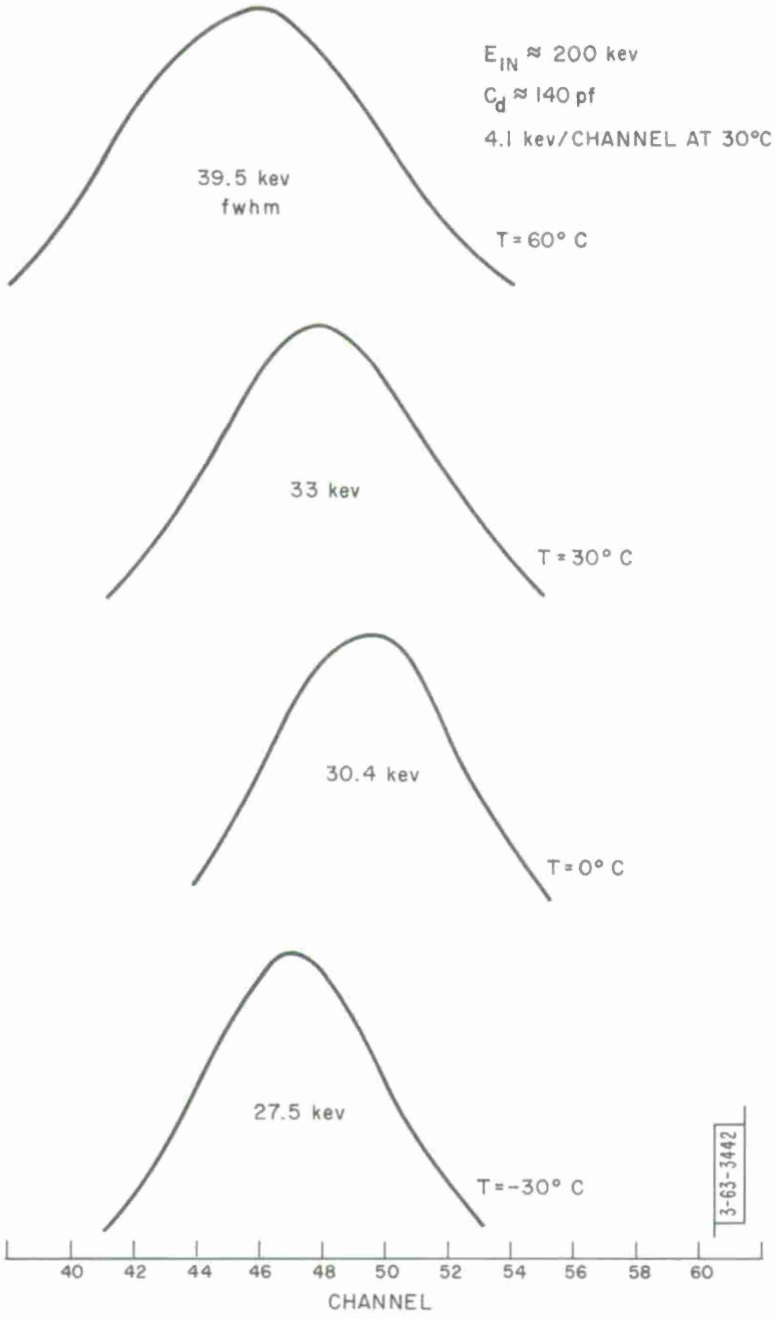

Fig. 27 Preamplifier Pulse Height Spectrum

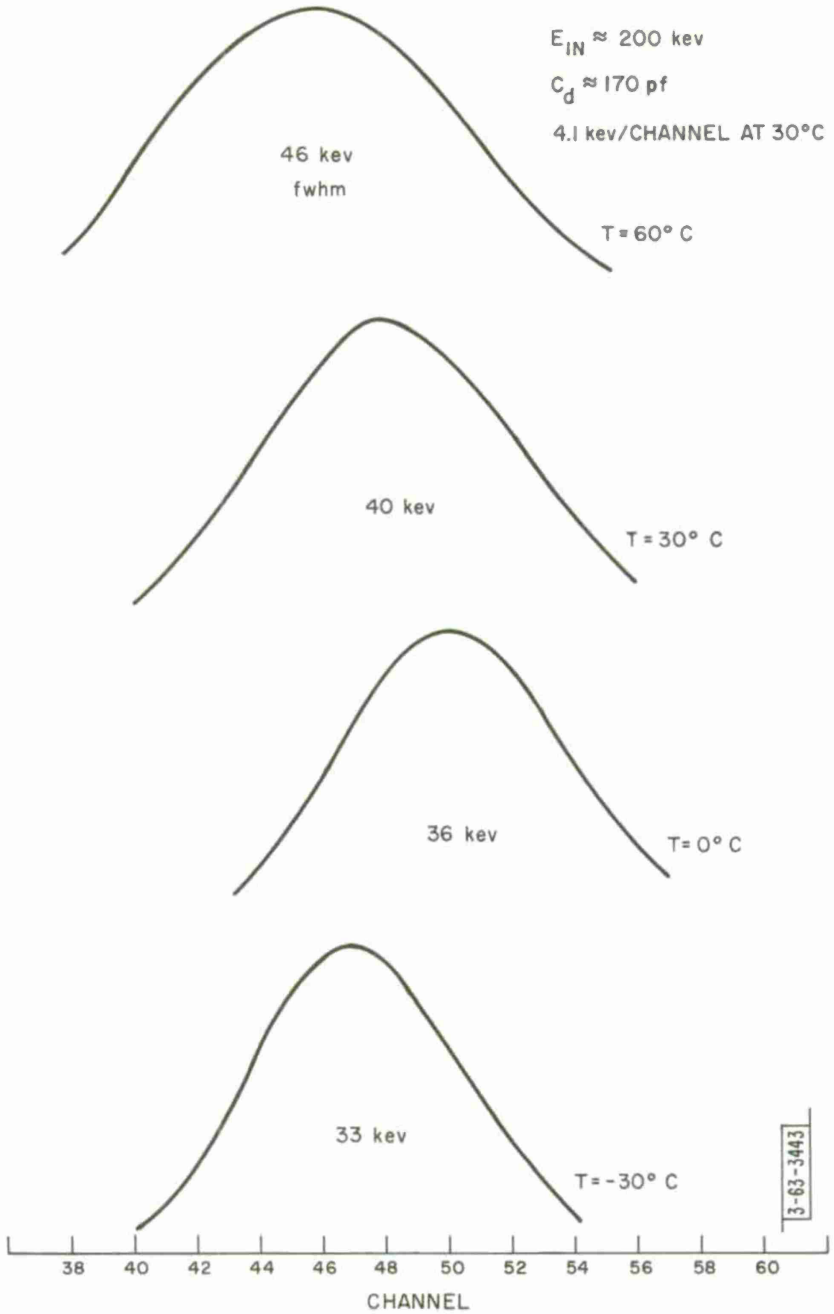

Fig. 28 Preamplifier Pulse Height Spectrum

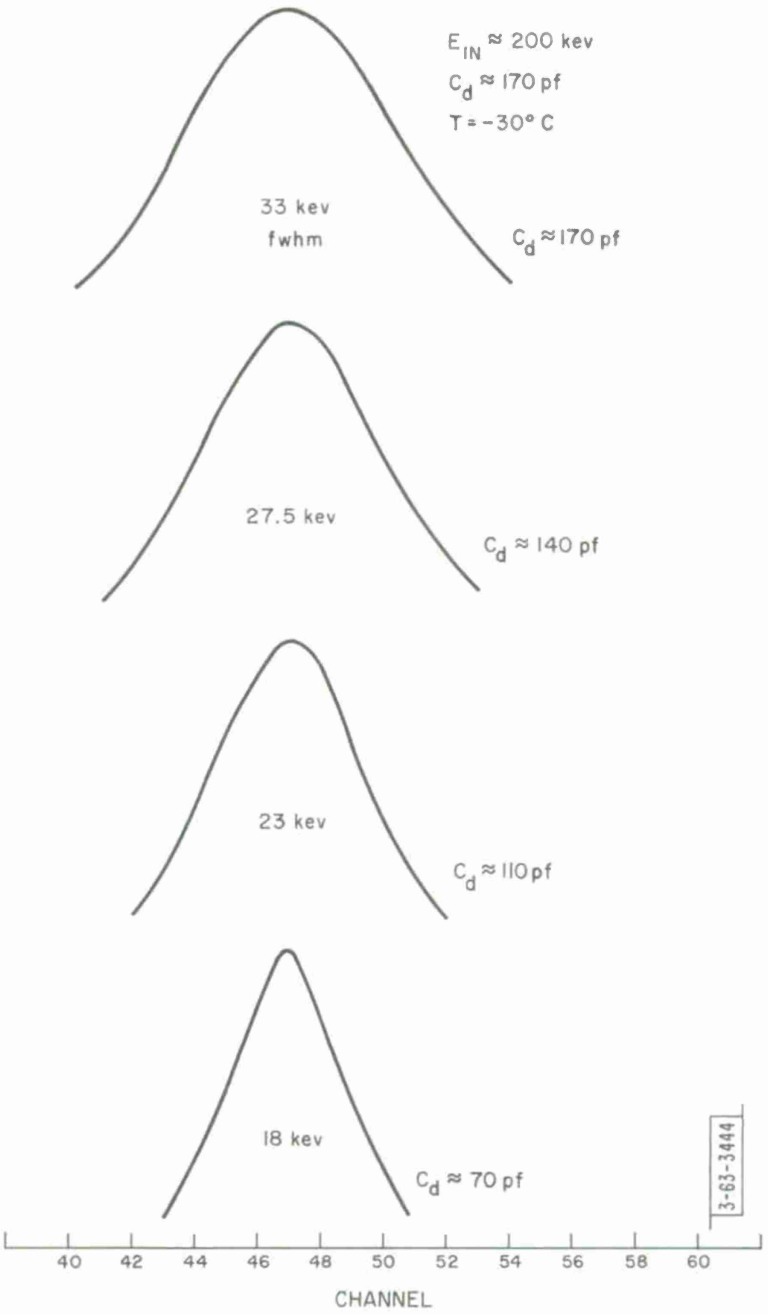

Fig. 29 Preamplifier Pulse Height Spectrum

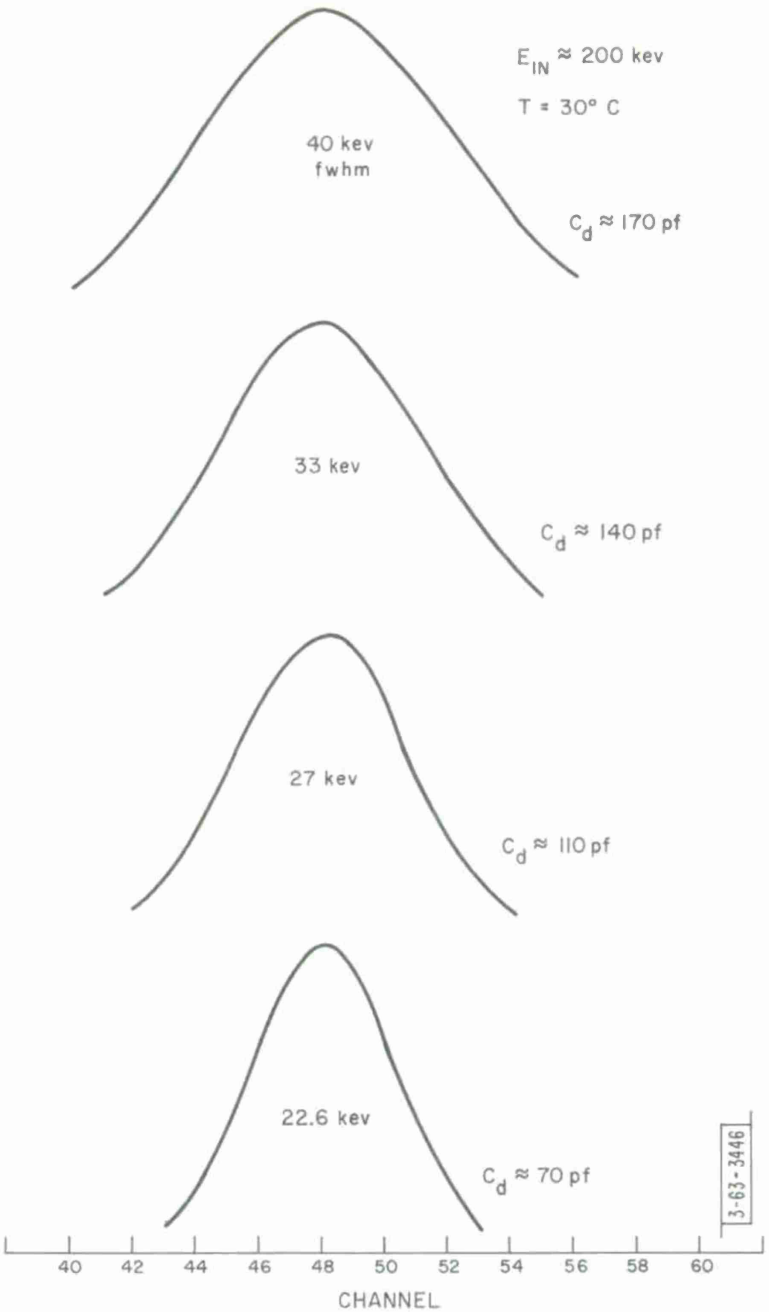

Fig. 31 Preamplifier Pulse Height Spectrum

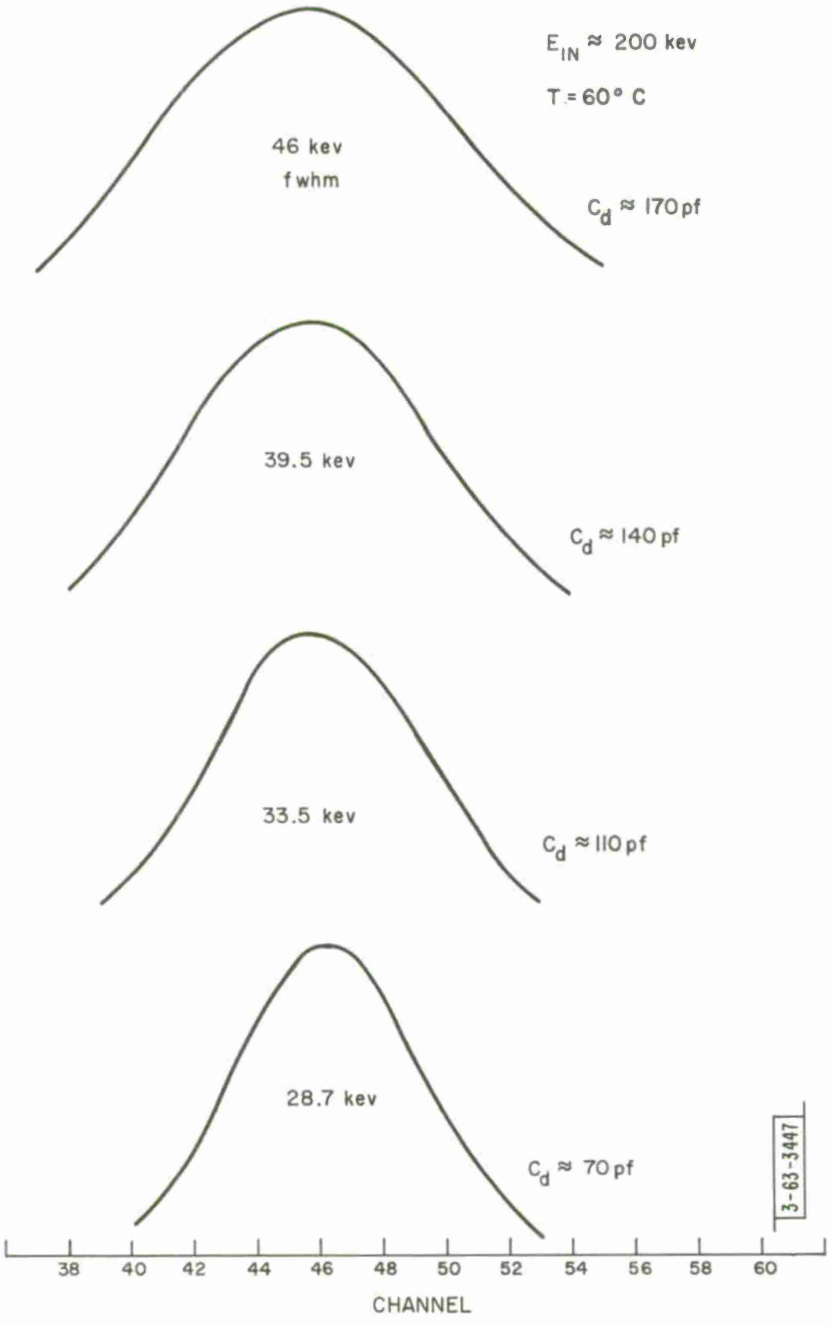

Fig. 32 Preamplifier Pulse Height Spectrum

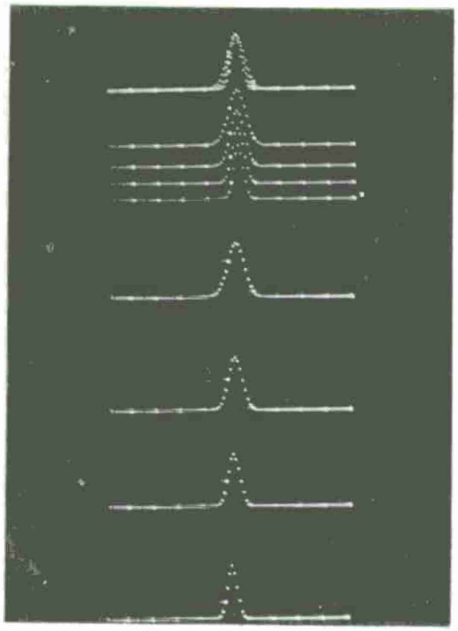

T = -30° C

COMPOSITE OVERLAY SHOWING PEAK INDEPENDENCE OF C_d

$C_d \approx 170$ pf

$C_d \approx 140$ pf

$C_d \approx 110$ pf

$C_d \approx 70$ pf

$E_{IN} \approx 200$ kev

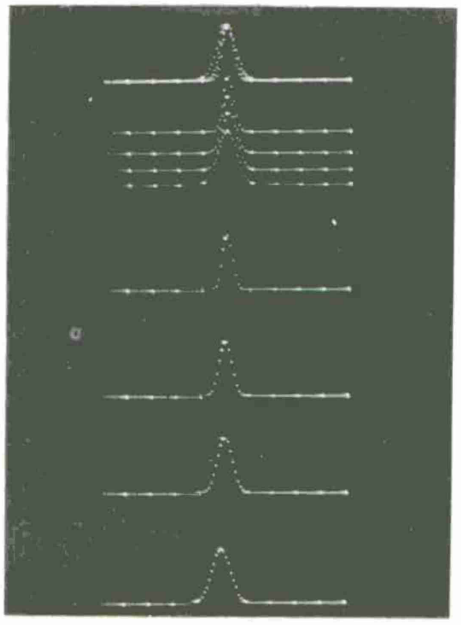

T = 0° C

COMPOSITE OVERLAY

$C_d \approx 70$ pf

$C_d \approx 110$ pf

$C_d \approx 140$ pf

$C_d \approx 170$ pf

-63-3448

Fig. 33 Pulse Height vs. Capacitance

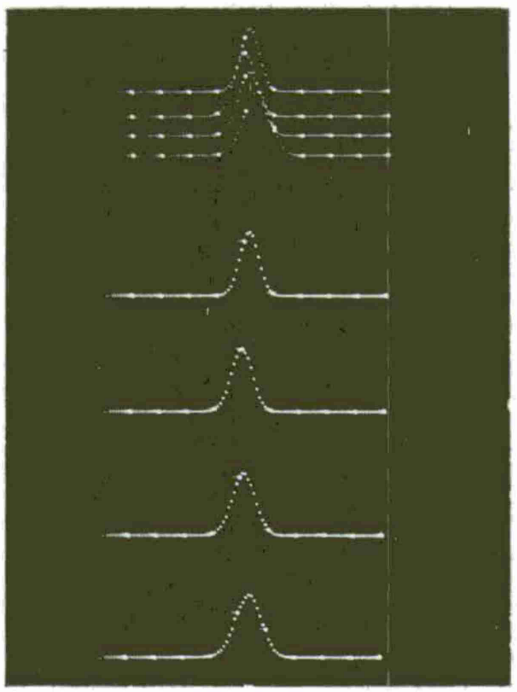

-63-3449

COMPOSITE OVERLAY OF SPECTRUMS AT
-30° C ; 0° C ; +30° C ; +60° C

T = -30° C

T = 0° C

$C_d \approx 170$ pf

T = +30° C

$E_{IN} \approx 200$ kev

T = +60° C

Fig. 34 Pulse Height vs. Temperature

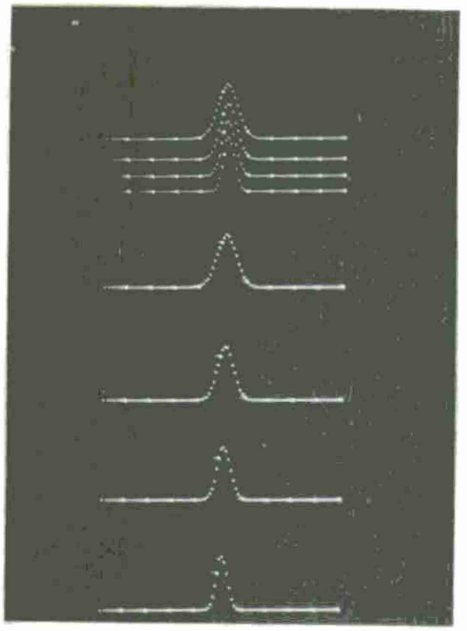

T = + 30° C

COMPOSITE OVERLAY

$C_d \approx 170$ pf

$E_{IN} \approx 200$ kev

$C_d \approx 140$ pf

$C_d \approx 110$ pf

$C_d \approx 70$ pf

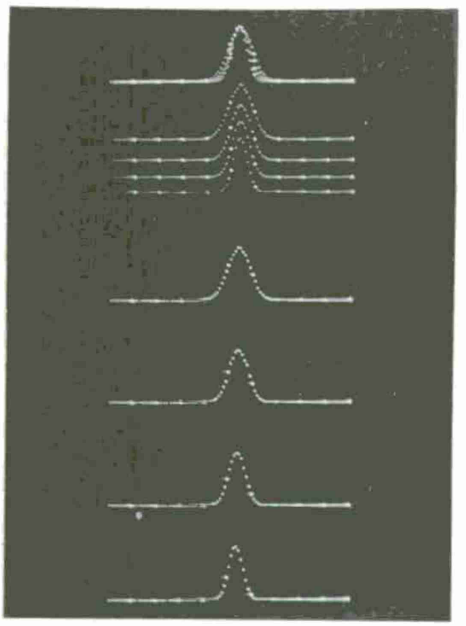

T = + 60° C

COMPOSITE OVERLAY SHOWING PEAK INDEPENDENCE OF CAPACITY

$C_d \approx 170$ pf

$C_d \approx 140$ pf

$C_d \approx 110$ pf

$C_d \approx 70$ pf

-63-3450

Fig. 35 Pulse Height vs. Capacity

Fairstein has proposed another method of measuring the noise linewidth. The output noise voltage is measured as V_n(rms). Next a known charge is deposited at the input, $Q_{in} = C_{in}V_{in}$, and then the resulting output voltage is measured at its peak, V_o peak. From these measurements the equivalent noise charge at the input can be determined.

$$Q_n(\text{rms}) = \frac{C_{in}V_{in}}{V_{o\ \text{peak}}} \quad V_n(\text{rms})$$

From this the fwhm energy can be found

$$E_{\text{fwhm}} = 2.35\, E_{\text{rms}} = 2.35 \frac{3.5}{q} Q_n(\text{rms})$$

However, a check of this analysis did not yield results in agreement with the measured values. For the parameters used in the measurement chain one should find that

$$E_{\text{fwhm}}\ (\text{kev}) = 0.7\ V_n(\text{mv, rms})$$

But as indicated in Fig. 36 it was found that

$$E_{\text{fwhm}}\ (\text{kev}) = 1.22\ V_n(\text{mv, rms})$$

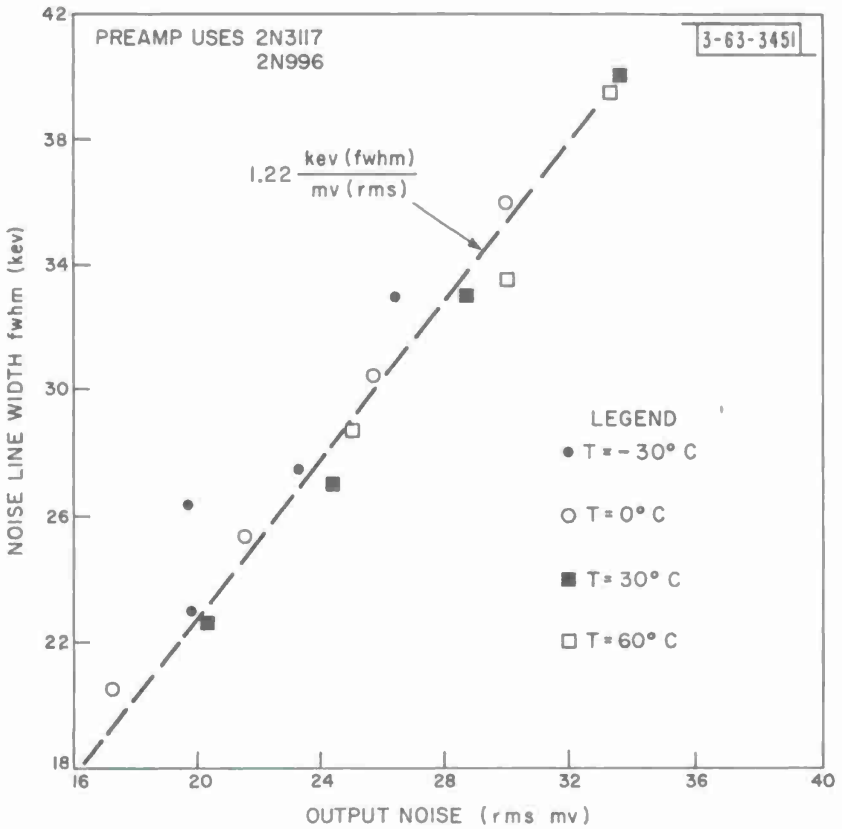

Fig. 36 Noise Characteristics

G. Construction Considerations

Needless to say the input stray capacity must be kept to a minimum. In the few breadboard designs attempted, ground plane printed circuit techniques proved very beneficial. Further improvement can be expected when integrated circuits are used in the measurement chain.

H. The Discriminator

A discriminator was studied and partially developed which would be triggered by a few millivolt change in input pulse height centered at some non-critical level near 100 mv. Figure 41 shows the present circuit and Fig. 42 indicates the signal required to trigger discriminator for various temperatures. It is seen that the required triggering signal varies less than 5 mv from +30°C to -30°C. This normally corresponds to a variation of electron energy of less than 10 kev. The temperature sensitive resistor in the bias circuit permits this flat response.

In standard operation Q_1 and Q_4 are off and Q_2 and Q_3 are on. Q_3 is in light saturation. When a negative pulse is applied with sufficient amplitude to offset the standby bias on the base of Q_1, then Q_1 conducts and reduces the required base current from Q_3. Q_3 comes out of saturation and the base voltage of Q_4 falls. As soon as this voltage is sufficient to turn Q_4 on, two positive feedback loops give regenerative action to finish turning the discriminator. The positive going pulse from the collector of Q_4 is coupled to the base of Q_3 to further turn it off; excess drive is damped by the diode to the $-V_3$ potential. The positive pulse is also coupled to the base of Q_2 to further turn it off, and supply an input to Q_5, the output buffer.

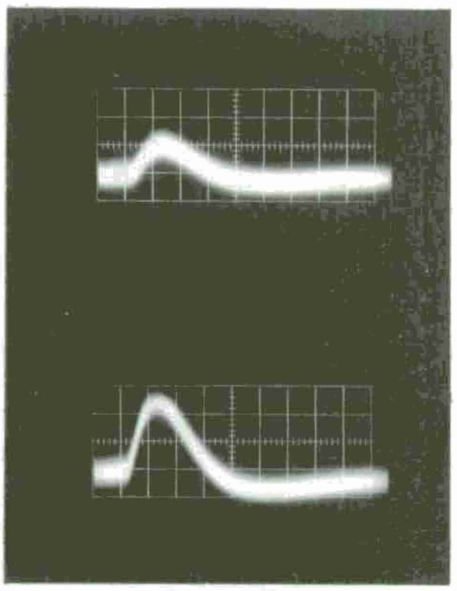

-63-3452

← 40 kev EQUIVALENT

VERTICAL 100 mv / DIV

HORIZONTAL 1 μsec / DIV

← 100 kev EQUIVALENT

SIMULATED DETECTOR CAPACITY:
$C_d \approx 110$ pf

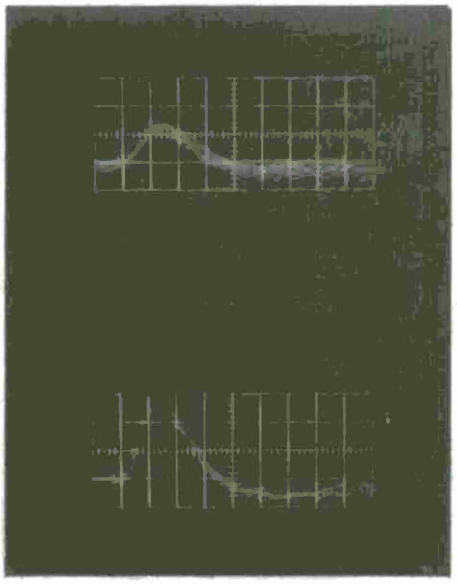

SAME TEST SIGNALS SHOWING
GRAININESS OF OUTPUT

Fig. 37 Test Signals

-63-3453

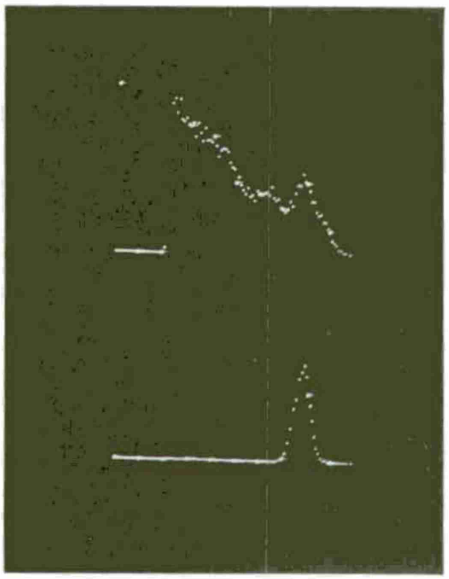

Ba^{133} SOURCE SHOWING PEAK AT
319 kev IN CHANNEL 78 FOR
4.1 kev / CHANNEL

A 5.3 mv TEST SIGNAL PEAKING AT
CHANNEL 78 FOR ≈ 60 kev / mv
FOR TEST SIGNALS

CHANNEL ⟶

Bi^{207} SOURCE SHOWING MAIN PEAK AT
972 kev

CHANNEL ⟶

Fig. 38 Pulse Height Spectrum Ba^{133} Source

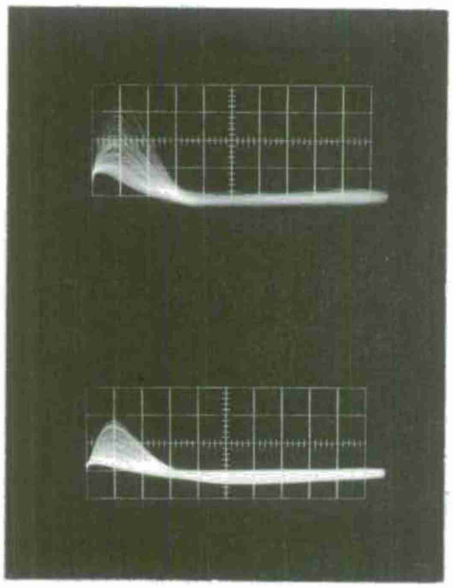

-63-3454

VERTICAL 0.2 VOLT / DIV

HORIZONTAL 1 μsec / DIV

VERTICAL 0.5 VOLT / DIV

NOTE THE 319 kev LINE NEAR ≈ 0.7 VOLT

THUS THE PREAMPLIFIER CONVERSION FACTOR IS $F_c \approx 2.3 \frac{\text{VOLT}}{\text{Mev}}$

Fig. 39 Preamplifier Output Waveforms for Ba^{133} Electron Source

The discriminator remains in this turned state until the base voltage of Q_2 decays back to steady state and thus turns Q_2 back on. This action steers the emitter current source away from Q_1, and thereby permitting its collector voltage to fall toward —6 volts with a time constant determined by the 10 pf and 100 K combination. This voltage falls only as far as the base emitter drop across Q_3 and then the circuit returns to its standby condition. The pertinent waveforms are shown in Fig. 43.

It should be pointed out that an adequate study of the best solution to the discriminator problem could not be completed due to lack of time on the part of this investigator. Further study and development should be continued.

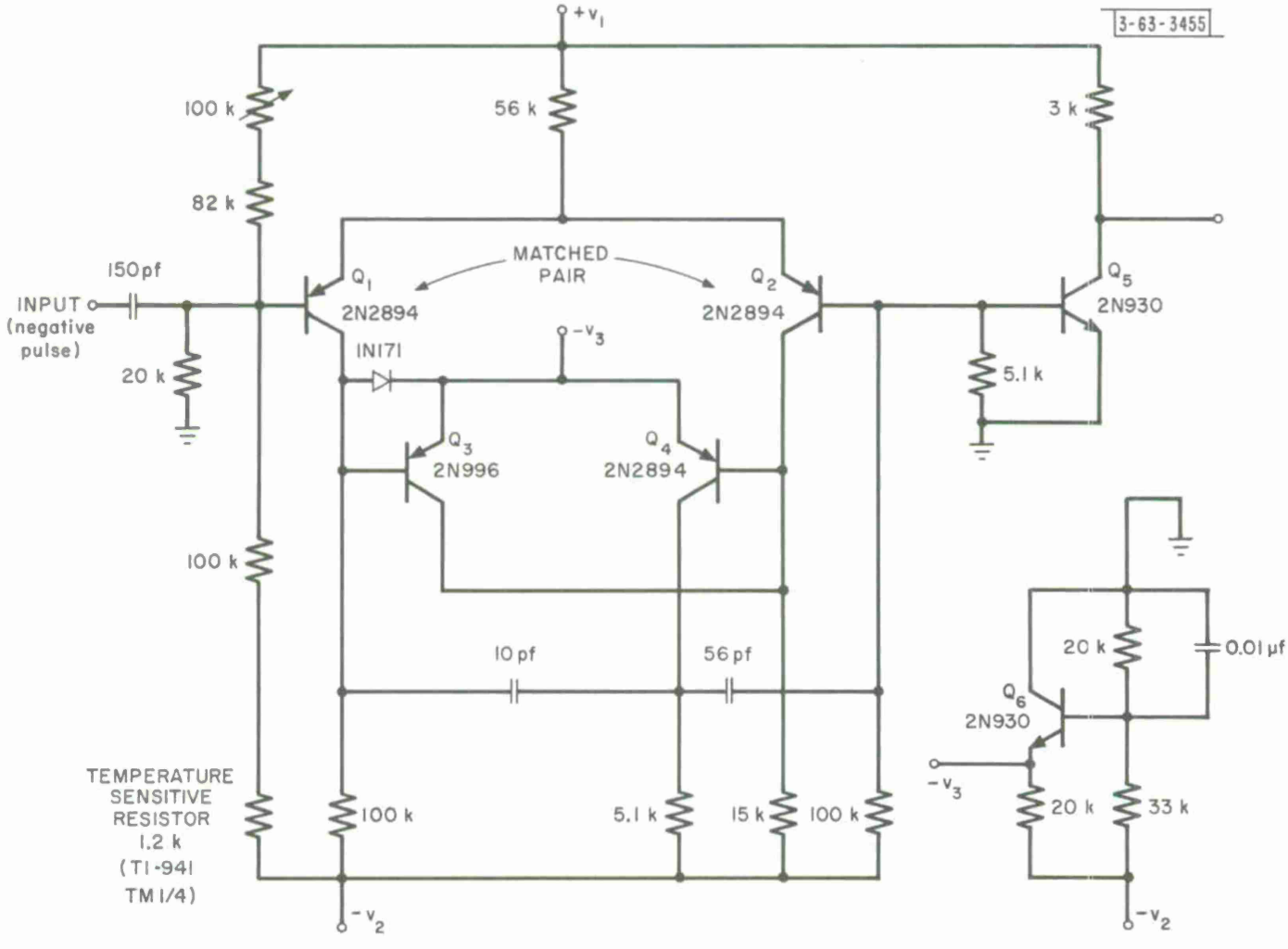

Fig. 40 Discriminator

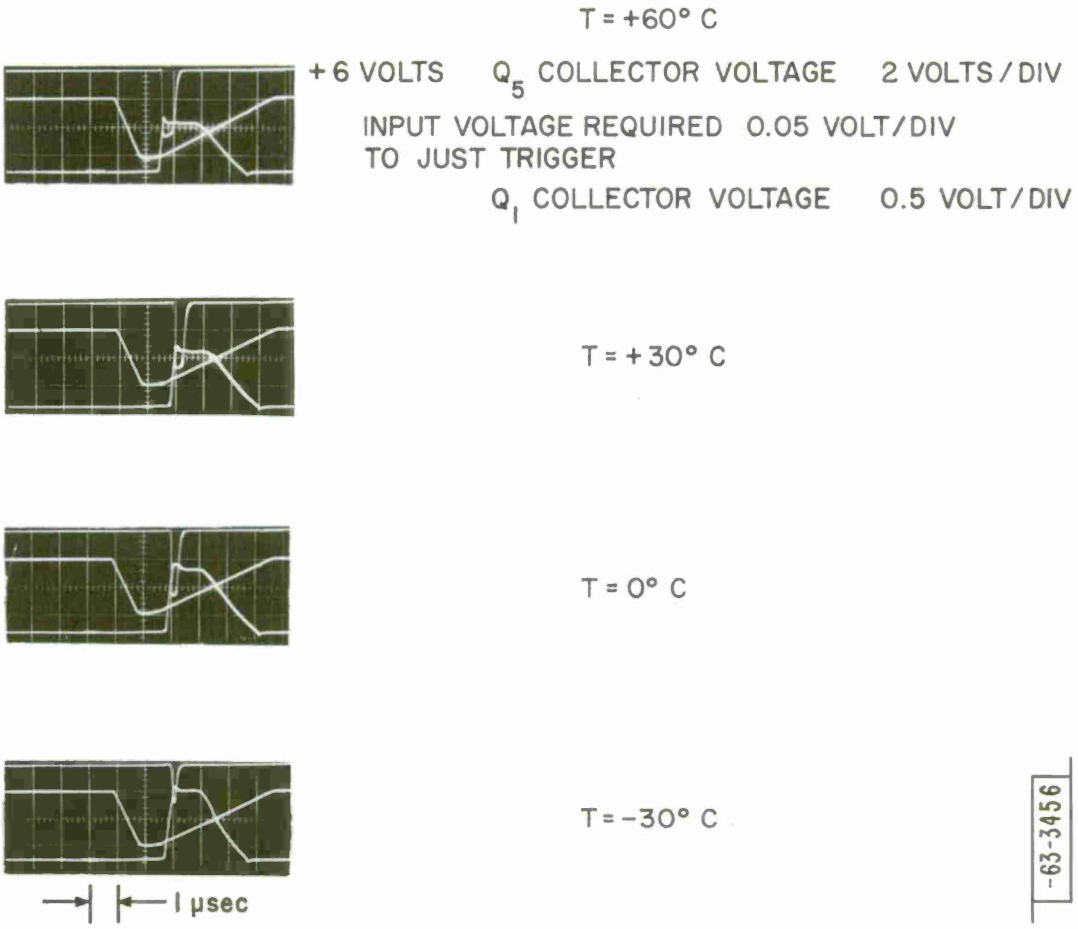

Fig. 41 Discriminator Waveforms for Various Temperatures

-63-3457

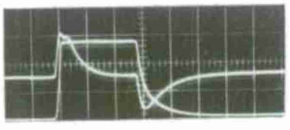

0 VOLTS Q_2 BASE VOLTAGE 0.5 VOLT/DIV

-6 VOLTS Q_4 COLLECTOR VOLTAGE 1 VOLT/DIV

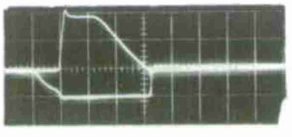

$-V_3$ VOLTS Q_1 COLLECTOR VOLTAGE 0.5 VOLT/DIV

$-V_3$ VOLTS Q_2 COLLECTOR VOLTAGE 0.5 VOLT/DIV

+6 VOLTS Q_5 COLLECTOR VOLTAGE 2 VOLTS/DIV

0 VOLTS Q_1 BASE VOLTAGE 0.2 VOLT/DIV

NOT TRIGGERING CONDITION

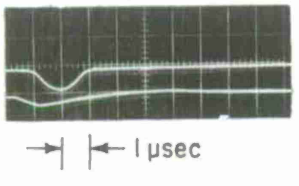

$-V_3$ VOLTS Q_2 COLLECTOR VOLTAGE 0.5 VOLT/DIV

Q_1 BASE VOLTAGE 0.2 VOLT/DIV

Fig. 42 Discriminator Waveforms at T = + 25°C

ACKNOWLEDGMENT

The author wishes to acknowledge the many helpful discussions with R. E. McMahon in formulating the design concepts of this experiment. His frequent assistance and guidance is gratefully appreciated.

DISTRIBUTION LIST

J. Binsack
R. M. Lerner
C. L. Mack
D. C. MacLellan
R. E. McMahon
J. Ryan
H. Sherman
A. G. Stanley

Group 63 Office - 10

DOCUMENT CONTROL DATA – R&D

(Security classification of title, body of abstract and indexing annotation must be entered when the overall report is classified)

1. ORIGINATING ACTIVITY *(Corporate author)*
Lincoln Laboratory, M.I.T.

2a. REPORT SECURITY CLASSIFICATION
Unclassified

2b. GROUP
None

3. REPORT TITLE
Proposed Electronic Systems for the LES Radiation Experiment

4. DESCRIPTIVE NOTES *(Type of report and inclusive dates)*
Technical Note

5. AUTHOR(S) *(Last name, first name, initial)*
Binsack, Joseph H.

6. REPORT DATE	7a. TOTAL NO. OF PAGES	7b. NO. OF REFS
20 July 1965	92	3

8a. CONTRACT OR GRANT NO.
AF 19(628)-5167
b. PROJECT NO.
None
c.
d.

9a. ORIGINATOR'S REPORT NUMBER(S)
TN 1965-5

9b. OTHER REPORT NO(S) *(Any other numbers that may be assigned this report)*
ESD-TDR-65-54

10. AVAILABILITY/LIMITATION NOTICES
None

11. SUPPLEMENTARY NOTES
None

12. SPONSORING MILITARY ACTIVITY
Air Force Systems Command, USAF

13. ABSTRACT

To study the electron radiation environment of the Lincoln Experimental Satellite (LES), an electron detecting telescope has been proposed by C. Mack, et al. This report presents the proposed electronic system for this radiation experiment. This system is the result of a summer study by the author.

The logical design of the electronic system is based on the use of a "hybrid counter" as the scaler. The "hybrid counter" employs the best features of both the "fixed time" and the "fixed count" scalers and can operate over a wide range of counting rates.

Coincidence logic is programmed within the experiment so that the telescope can monitor the electron flux for energies from 60 kev to 10 mev with counting rates from 100,000 counts/sec down to 0.1 count/sec. The design of a charge sensitive solid state preamplifier and measurement chain is detailed. The integrating and differentiating time constant is set at 0.5 μsec, and a noise linewidth of 27 kev (fwhm) is achieved at 30°C with a simulated input capacitance of 100 pf.

14. KEY WORDS
LES electronic systems radiation effects